COLLISION BETWEEN FRACTIONAL SOLITONS IN FIBRE LASERS

TANDIN ZANGMO

A Thesis Submitted to the Graduate School of Naresuan University
in Partial Fulfillment of the Requirements
for the Master of Engineering in Electrical Engineering
2023

COLLISION BETWEEN FRACTIONAL SOLITONS IN FIBRE LASERS

TANDIN ZANGMO

A Thesis Submitted to the Graduate School of Naresuan University
in Partial Fulfillment of the Requirements
for the Master of Engineering in Electrical Engineering
2023
Copyright by Naresuan University

Thesis entitled "Collision between fractional solitons in fibre lasers"

By Tandin Zangmo

has been approved by the Graduate School as partial fulfillment of the requirements

for the Master of Engineering in Electrical Engineering of Naresuan University

Oral Defense Committee

.... Chair
(Associate Professor Athikom Roeksabutr, Ph.D.)

.... Advisor
(Associate Professor Thawatchai Mayteevarunyoo, Ph.D.)

.... Internal Examiner
(Associate Professor Surachet Kanprachar, Ph.D.)

.... Internal Examiner
(Assistant Professor Sommart Sang-ngern, Ph.D.)

Approved

....
(Associate Professor Krongkarn Chootip)
Dean of the Graduate School

Title	COLLISION BETWEEN FRACTIONAL SOLITONS IN FIBRE LASERS
Author	Tandin Zangmo
Advisor	Associate Professor Thawatchai Mayteevarunyoo, Ph.D.
Academic Paper	M.Eng. Thesis in Electrical Engineering, Naresuan University, 2023
Keywords	Fractional nonlinear Schrödinger equations; Riesz fractional derivative; group-velocity dispersion; Kerr nonlinearity; wavelength-division multiplexing; inelastic collisions of solitons; two-component solitons

ABSTRACT

In this study, a framework of fractional nonlinear Schrödinger equations (FNLSEs) is modelled that utilizes the effective fractional group-velocity dispersion (FGVD), which was recently provided to the experiment, to model the co-propagation of optical waves carried by distinct wavelengths in fibre-laser cavities. The FGVD terms are denoted in the FNLSE system through Riesz derivatives, each accompanied by its corresponding Levy Index (LI). The FNLSEs, which comprise self-phase modulation (SPM) nonlinearity, are coupled by cross-phase modulation (XPM) terms and separated by a group-velocity mismatch (rapidity). We examine collisions and bound states of solitons in the XPM-coupled system utilizing systematic simulations, altering the LI and GV mismatch. Collisions between solitons can result in rebound, conversion of single-component solitons into two-component ones, merger into a breather, and elastic effects. Additionally, families consisting of stable two-component soliton-bound states are generated, exhibiting an intermediate rate of acceleration between the two components.

ACKNOWLEDGEMENTS

It would not have been feasible for me to complete this thesis, "Collision between fractional solitons in fibre lasers," without the kind assistance of a network of acquaintances, both personal and professional. First and foremost, the Royal University of Bhutan (RUB) and Naresuan University (NU) have my profound gratitude and sincere appreciation for allowing me to pursue a master's degree in electrical engineering (Communication Engineering). In addition, I would like to extend my gratitude to the Department of Electrical Engineering, Faculty of Electrical and Computer Engineering, Naresuan University, Thailand, for fostering an environment conducive to my research and studies.

Without expressing appreciation to my direct supervisor, Associate Professor Dr. Thawatchai Mayteevarunyoo, the goal of this acknowledgement would not have been achieved. I am deeply grateful to the professor for providing me with this fascinating and pertinent research topic. Special appreciations are extended for all productive talks, important recommendations, and critical remarks. Furthermore, I would like to express my gratitude to the Professor for his unwavering support and diligent approach, both of which significantly impacted my coursework and my trajectory in life.

Professor Boris A. Malomed from Tel Aviv University, Tel Aviv, Israel deserves my heartfelt gratitude and appreciation for his instrumental contributions to this research in terms of intellectual input and wealth of knowledge.

I would like to thank Associate Professor Dr. Surachet Kanprachar and Assistant Professor Dr. Sommart Sang-Ngern for serving as an internal examiner and Associate Professor Dr. Athikom Roeksabutr for serving as an external examiner for useful constructive comments.

I also want to express my gratitude to my parents and siblings for their unwavering support and encouragement, which have been instrumental in helping me overcome challenges and embrace valuable opportunities. I want to express my gratitude to my friends for consistently assisting and supporting me in sharing thoughts when necessary.

Tandin Zangmo

TABLE OF CONTENTS

LIST OF FIGURES

Page

ABBREVIATIONS

WDM	=	Wavelength Division Multiplexing
FOC	=	Fibre Optic Communications
GVD	=	Group Velocity Dispersion
FGVD	=	Fractional Group Velocity Dispersion
CD	=	Chromatic Dispersion
1D	=	One Dimensional
LI	=	Levy Index
QM	=	Quantum Mechanics
FQM	=	Fractional Quantum Mechanics
SPM	=	Self-Phase Modulation
DCF	=	Dispersion Compensation Fiber
SMF	=	Single Mode Fiber
LASERS	=	Light Amplification by Simulated Emission of Radiation
CPM / XPM	=	Cross Phase Modulation
FWM	=	Four-Wave Mixing
NLSE	=	Nonlinear Schrödinger Equation
TOD	=	Third Order Dispersion
PDE	=	Partial Differential Equation
ODE	=	Ordinary Differential Equation
NPDE	=	Nonlinear Partial Differential Equation
FSE	=	Fractional Schrödinger Equation
FPDE	=	Fractional Partial Differential Equation
FNPDE	=	Fractional Nonlinear Partial Differential Equation
FNLSE	=	Fractional Nonlinear Schrödinger Equation
TFSE	=	Time-dependent Fractional Schrödinger Equation
SFSE	=	Space-dependent Fractional Schrödinger Equation
NLSE	=	Nonlinear Schrödinger Equation

NLEE	=	Nonlinear Evolution Equation
FT	=	Fourier Transform
IFT	=	Inverse Fourier Transform
KdV	=	Korteweg-de Vries
SOM	=	Squared Operator method
MSOM	=	Modified Squared Operator method
SSFM	=	Split Step Fourier method
FT	=	Fourier Transform
IFT	=	Inverse Fourier Transform
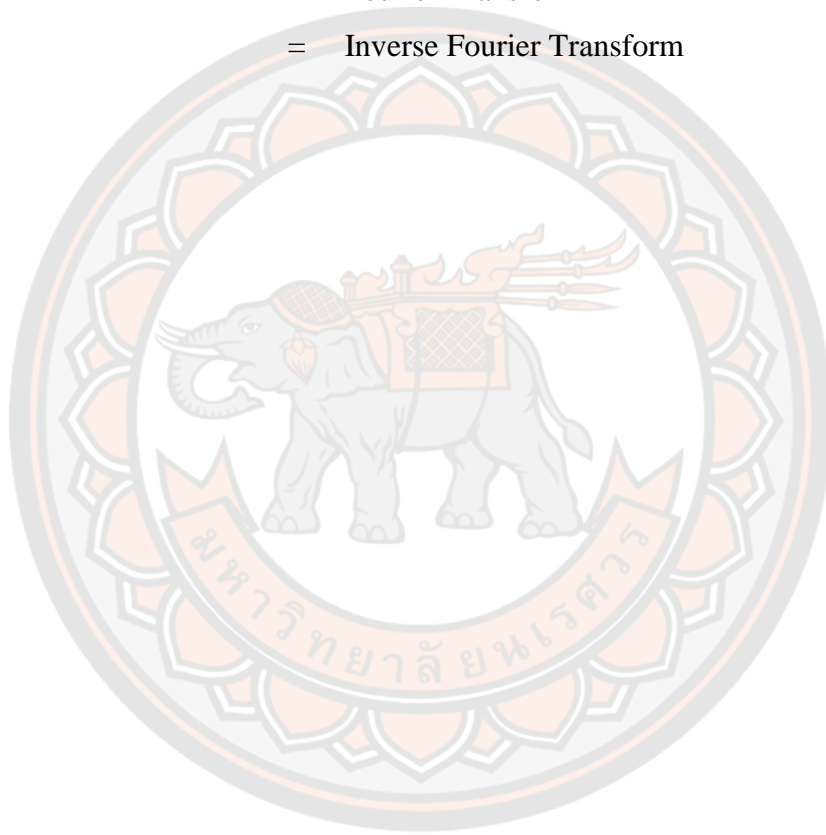
NOMENCLATURE FOR SYMBOLS

Symbol	Meaning
γ	Nonlinear coefficient
λ	Wavelength
α	Levy Index
β_2	Second Order Dispersion
A	Optical intensity or amplitude
ψ	Wave function
τ	Time
V	Potential
p	momentum
$\hbar$	Reduced Planck's constant
m	Mass of the particle
β_k	kth order GVD
k	Wave number
z	Propagation distance
E	The energy content of the soliton

CHAPTER I

INTRODUCTION

1.1 Background

An essential direction in theoretical and experimental studies in modern-day physics is the creation and studies of artificial media which realize various "exotic" properties that are impossible in natural systems. Well-known examples are metamaterials and meta-surfaces in photonics, which make it possible to demonstrate unusual linear and nonlinear properties of optical and plasmonic waves, such as negative refraction, cloaking, etc. (Keren-Zur et al., 2018). A new remarkable result in this area is the creation of photonic counterparts of topological insulators (Khanikaev et al., 2013).

Another direction in the development of artificial settings makes use of Bose-Einstein condensates (BECs) in atomic gases. They make it possible to emulate various fundamental effects which are known in much more complex forms in condensed-matter physics, such as spin-orbit coupling (SOC) (Zhai, 2015).

A specific class of artificial optical media features effectively fractional paraxial diffraction. First, this concept was introduced in quantum mechanics, as the fractional Schrödinger equation for the wave function of a particle moving by random jumps (Lévy flights) by (Laskin, 2000).

$$i\frac{\partial\psi}{\partial t} = \mathcal{D}_\alpha \left(-\frac{\partial^2}{\partial x^2}\right)^{\alpha/2} \psi + V(x)\psi \tag{1}$$

where α is the Levy index $(1 < \alpha \le 2)$, $\mathcal{D}_\alpha$ is a scale constant, $V(x)$ is the external potential, and $\psi = \psi(x,t)$ is the particle wave function. In equation (1), the kinetic term in the Hamiltonian is represented by the quantum Riesz derivative (fractional Laplacian) of order α, which is defined by (Kilbas et al., 2006):

$$\left(-\frac{\partial^2}{\partial x^2}\right)^{\alpha/2} \psi(x) = \frac{1}{2\pi} \iint_{-\infty}^{\infty} dp\, d\xi |p|^\alpha \psi(\xi) \exp\left[ip(x-\xi)\right] \tag{2}$$

The ordinary Schrödinger equation is obtained in the limiting case $\alpha = 2$. The realization of equation (1) from (Stickler, 2013) is based on lattice dynamics in Levy crystals. While the experimental realization of fractional quantum mechanics is missing, the well-known similarity of the quantum-mechanical Schrödinger equation to the paraxial wave-propagation equation in optics suggests a possibility of simulating FSE in optics (Longhi, 2015). In this context, fractional diffraction may be implemented by transforming the spatial structure of the light beam into its Fourier counterpart, applying the fractional diffraction in its straightforward form in the Fourier layer, and then transforming the result back into the spatial structure. Very recently, this possibility was realized experimentally in the form of fractional dispersion in fibre lasers (Liu et al., 2023).

Fractional Calculus has gained considerable recognition and growth in the domains of science and engineering owing to its applications in fields such as Quantum Mechanics (QM), fluid dynamics, thermal dynamics, diffusion, material science and Schrodinger equations to name a few (Miller & Ross, 1993; Nishimoto, 1984; Oldham & Spanier, 1974; Ortigueira, 2011). Differential Equations of many kinds, including differential equations with fractional order and their extensions, have been solved by using fractional calculus operators and their generalizations (Alhorani & Khalil, 2018; Diethelm & Ford, 2002; Lakshmikantham & Vatsala, 2008; Podlubny, 1999; Vázquez et al., 2011). Multiple studies (Alshehry et al., 2022; Chen & Jiang, 2018; Feng & Meng, 2017; Feng & Ma, 2023; Kurt et al., 2019; Odabasi & Mısırlı, 2018; Pu et al., 2014; Wang & Zheng, 2019) have examined both Fractional Partial Differential Equations (FPDE) and Nonlinear Partial Differential Equations (NPDE) which is a special case of FPDEs for providing numerous analyses in nonlinear optics, fluid dynamics, optical fibre, signal processing and so on.

In recent decades, numerous investigations have been conducted on optical soliton (Cao & Dai, 2021; Chen et al., 2019; Felmer et al., 2012; Mehboob et al., 2019; Qiu et al., 2020). The study of optical soliton is a fascinating subject that involves examining the propagation of solitons across nonlinear optical fibres (Agrawal, 2000). Optical solitons are confined electromagnetic waves that exist in a nonlinear dispersive medium and maintain a constant intensity by balancing the effects of Group Velocity

Dispersion (GVD) and nonlinear effects. The dynamics of nonlinear wave propagation are governed by the Nonlinear Schrodinger Equations (NLSE) and to obtain analytical solutions of these Nonlinear PDEs are vital for studying nonlinear processes. Numerous methods have been developed to derive solutions over the years such as the trial solution method (Biswas et al., 2016), the sine-Gordon expansion method (Bulut et al., 2018), solitary wave ansatz (Bhrawy et al., 2014), the functional variable methods (Rezazadeh, 2018), the inverse scattering methods (Ghosh & Nandy, 1999), and the Kudryashov-expansion method (Alquran et al., 2019), etc.

1.2 Problem statement

A lot of research on optical solitons has been done on integer-ordered (non-fractional) properties of the medium, where the solitons' dispersion and refractive index either change linearly with wavelength or stay the same. The concept of fractionalizing the medium in optical and nonlinear settings has only been around for two decades, and much is still unknown, which only attracts attention.

The study of optical solitons in a fractional medium is an insufficiently explored area with limited comprehensive investigation in the current literature. In application point of view, experimental realisation of the fractional soliton in a standard single mode fibre (SMF) and optical resonator cavities have been performed by (Chen et al., 2019; Esen et al., 2018; Fujioka et al., 2010; Longhi, 2015; Mehboob et al., 2019; Wu et al., 2020), however, the application has not been extended to active optical devices such as fibre lasers.

The fibre laser in this research is intentionally treated as a passive device to simplify the analysis of fractional soliton propagation dynamics. By ignoring the complications associated with gain and loss mechanisms, the mathematical treatment becomes more manageable, allowing for a more focused exploration of the FNLSE's dispersive and nonlinear effects. In addition, it also allows to isolate and comprehend the fundamental behaviour of fractional solitons within the fibre medium prior to introducing additional complexities while this idealised passive device model may not fully capture the complexities of a real-world fibre laser, it is an important step towards a more complete understanding of fractional soliton propagation in active systems.

As a result, this study uses this simplified passive device formulation as a basic framework, laying the door for possible future developments that include gain and loss dynamics.

Additionally, the majority has explored the space or spatiotemporal (space-time) aspects of the fractional soliton with only a few in the temporal domain in recent years which is another reason to carry out this study in temporal domain to learn more insights.

The literature lacks comprehensive research on the existence and interaction (collision) events of many fractional solitons within a cavity laser emulating a WDM environment. Investigating this topic has the potential to greatly enhance our understanding in a broader field and could even lead to improvements in its practical uses beyond photonics. This gap is filled by conducting thorough numerical simulations utilising the WDM framework by using two fractional solitons and investigating their dynamical behaviour when co-propagating with and without the effects of XPM. Two fractional solitons are defined as u and v component or in optical communication, it can be seen as two wavelengths or channels. Although in this study, for the simplicity, it is in normalized form and assumed to have same solution profile.

The study aims to achieve a comprehensive understanding of the fractional soliton in fractional medium and how different it is compared to the standard system with integer-order derivatives. The analysis examines various characteristics such as fractional order, soliton amplitude, soliton spacing, and soliton phase. Here, the numerical method is employed to solve the FNLSE equations, and, through numerical simulation, the results are presented graphically by varying the parameters. The Modified Squared Operator method is an iteration method that exhibits fast convergence, is time-efficient, and provides accurate results (finding solutions). Furthermore, it is indifferent to dimensions and suitable to a broad variety of solitary and soliton waves due to which they are termed as universally convergent technique by Yang in 2007. Using Split Step Fourier Method for direct simulation is another significant part of numerical approach as its very easy to implement and faster and accurate method apart from being a popular technique especially for studies related to fractional dimensions and in optical domain.

Additionally, it uncovers some novel characteristics and provides opportunities for manipulating fractional solitons in fibre lasers. Moreover, this study makes a substantial contribution to the progress of fractional calculus and nonlinear optics, perhaps influencing other disciplines that include fractional-order systems.

1.3 Aims and Objectives.

1.3.1 Aim:

To study collision between fractional solitons in the fibre lasers using numerical simulations using the Split-Step Fourier (SSF) method. The model is described by coupled Fractional Nonlinear Schrödinger Equations (FNLSE) which is relevant for the system with two different carrier wavelengths (as an element in the WDM setup)

1.3.2 Objectives:

To fulfil the above aim, this study has the following objectives.

1. Introduce the model equation (FNLSE) describing the co-propagation of two fractional solitons in fibre-laser cavities with fractional dispersion (FGVD) and Kerr nonlinearity (SPM and XPM).

2. Study the dynamics of fractional solitons with and without the direct effect of XPM on the co-propagating solitons by separating studies into two cases.

3. Find fractional soliton solutions in both the cases by adopting Modified Square Operator Method (MSOM) as an iterative method followed by direct simulation using Split Step Fourier Method.

4. Compare the numerically found fractional soliton solutions of each case with the available analytical solutions of each case at $k = 1$ and $\alpha = 2$ which corresponds to a system described by ordinary NLSE (standard system).

5. Using systematic simulations with different α and velocity mismatch (c), examine collisions and bound states of solitons in the XPM-coupled system.

1.4 Purpose and Significances of Study

The current study uses a numerical simulation approach using MATLAB software to simulate and generate visual and graphical illustrations to demonstrate the effect of collisions between two channels in a fibre laser. The fibre laser here is the

fractional nonlinear medium through which multiple soliton channels will propagate and collide. The equations governing the propagation of these fractional solitons are described by Fractional Nonlinear Schrödinger Equations (FNLSE) which will be solved by using Split Step Fourier Transform.

Studying the dynamic behaviour of optical solitons continues to fascinate researchers from diverse fields such as fluid mechanics, plasma, nonlinear optics, photonics, quantum mechanics, thermodynamics etc. After (Longhi, 2015) introduced the applicability of the Fractional Schrödinger Equation (FSE) in optics, it opened the door to new possibilities in fibre optic communication and the development of optical components and devices. Knowing how to manipulate and control the fractional solitons in an optical communication system gives insights to optimize and enhance the performances.

In a nonfractional medium, when multiple channels co-propagate with proximity, due to nonlinear effects such as Self Phase Modulation and Cross Phase Modulation (XPM), collision of solitons takes place giving rise to many undesired phenomena. Collision dynamics in a fractional medium is a relatively new idea with no record of previous studies.

The study expands its existing knowledge base beyond optics into various science and engineering domains in understanding complex systems and processes in a broad sense. A comprehensive understanding of collision dynamics of the fractional soliton can contribute to all future researchers in refining the idea and concept. The design and development of efficient optical devices in the fractional medium could be of huge benefit.

1.5 Scope of study

The study seeks to examine the impacts of soliton collisions in a fibre laser. Fibre lasers are active optical devices renowned for their versatile uses in the generation, propagation, and amplification of light beams. It can be described as a fusion of rare-earth-doped fibre amplifier (DFA) and transmission fibre, specifically designed to handle high-power transmissions. The main objective is to examine the collision caused by Kerr nonlinearity in a WDM environment while considering the effects of SPM and XMP between two channels.

The mathematical equation employed to represent it is a fractional extension of the Nonlinear Schrödinger Equation (NLSE) incorporating fractional derivatives. The conventional nonlinear Schrodinger equation features a derivative of integer order. However, when this integer-order derivative is substituted with fractional-order (non-integer) derivatives, it gives rise to a fractional nonlinear Schrödinger equation (NLSE). The optical soliton can be fractionalized in various aspects, such as its nonlinearity, refractive index, medium, and dispersion. In this scenario, the consideration is exclusively in the temporal domain, meaning only time domain dispersion. Here, the substitution of the conventional second-order derivative of the nonlinear Schrödinger equation (NLSE) with a fractional derivative of order α.(Fujioka et al., 2010) conducted a study where they investigated the temporal propagation of solitons in a fractional medium. They achieved this by incorporating higher-order dispersion and higher-order nonlinearity, however, multichannel was not mentioned.

The FNLSE is solved using the SSFT method to obtain numerical results. Additionally, numerical simulation is conducted to validate these results and visually illustrate the collision events. Within the WDM setting, the nonlinear effects that arise include Self-Phase Modulation (SPM) and Cross-Phase Modulation (XMP), which exhibit soliton characteristics. Additionally, the specific parameters of the Split-Step Fourier Transform (SSFT) method are employed to evaluate these events. The present study, being the first of its kind, focuses on design simplicity and therefore excludes the consideration of external potential, higher-order dispersion, loss, amplification (gain), higher-order nonlinearity, FWM effects, and different solitons in two channels. These aspects are part of the conceptual framework in nonlinear optics and are commonly used in applications within fibre laser devices. It is worth noting that no prior study has been conducted on this idea.

1.6 Organization of the Thesis

The remainder of this thesis is structured as follows:

1. Chapter 2: The literature review provides a comprehensive overview of the fractional Schrödinger equations in linear systems with its generalized extension in time and space variables. The nonlinear extension of FSE known as FNLSE is explored in context with optics and optical systems in terms of optical solitons in the fractional

medium. The methods to solve and study the collisions between two fractional solitons using modified squared operator methods are discussed along with numerical simulation methods using Split Step Fourier methods.

   2. Chapter 3: Methodology describes the process of carrying out the study by developing the mathematical model by incorporating FNLSE with nonlinear effects. The solution of the solitons will be obtained by solving the FNLSE with nonlinear effects (SPM and XPM) using MSOM methods and numerical simulation will be performed by MATLAB for the visual realization of the solution for various values of LI and GV mismatch.

   3. Chapter 4: Computational simulation is performed to investigate the effects of a collision between two fractional solitons. Graphical illustrations of the results are presented, and the summary of collisions is presented.

   4. Chapter 5: Conclusion and future work summarise the key contribution and outline potential areas for future research.
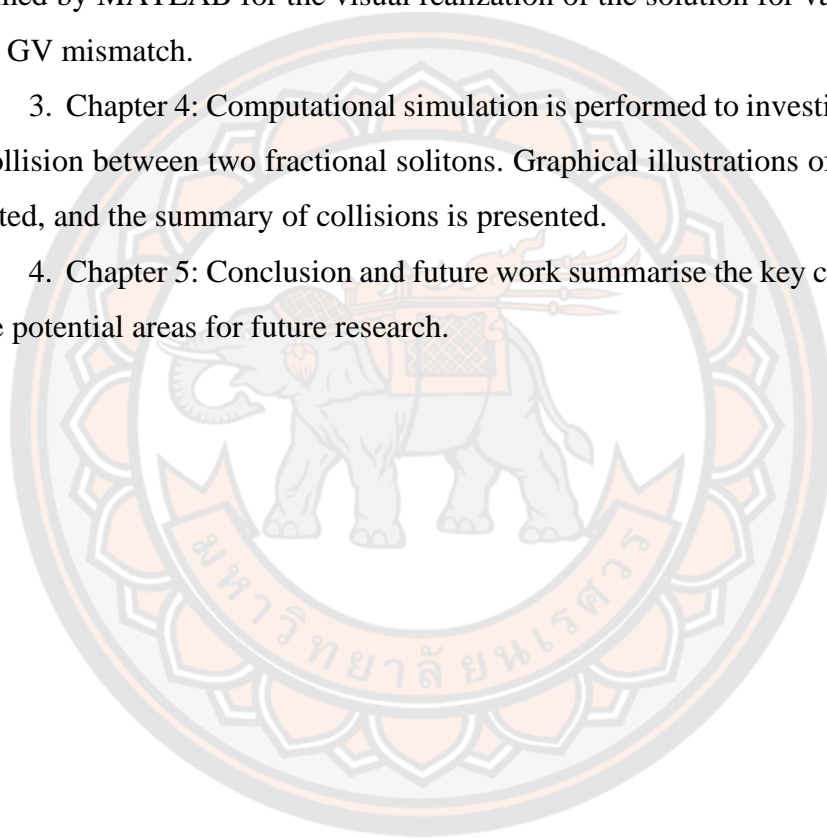
CHAPTER II

LITERATURE REVIEW

2.1 Fractional Schrödinger Equation in spatial domain

Fractional Schrödinger Equation (FSE) with a space derivative of order α in place of the second order ($\alpha = 2$) space derivative in a standard wave equation becomes Space Fractional Schrödinger Equation (SFSE). Path integrals over Brownian motion are based on the Gaussian distribution of all possible paths used by (Feynman & Hibbs, 1965) to derive the classical (non-fractional) Schrödinger Equation as a basic wave equation to describe the dynamics of a system through a wave function. One Dimensional (1D) of the SE is given as

$$i\hbar \frac{\partial \psi}{\partial t} = -\frac{\hbar^2}{2m}\frac{\partial^2 \psi}{\partial x^2} + V(x)\psi, \tag{3}$$

where $\psi = \psi(x, t)$ is the wave function, i is the imaginary unit, $\hbar$ is the reduced Planck's constant, $V(x)$ is the external potential and m is the mass of the particle. The first term on the left side of the equation (3) is the first-order time derivative and the first term on the right is the second-order space derivative. The second term on the same side is the external potential.

Fractionalizing the Standard Schrödinger Equation by Laskin led to the fractionalization of Quantum Mechanics (QM) into Fractional Quantum Mechanics (FQM) (Laskin, 2000; Laskin, 2002, 2008). He formulated the Space Fractional Schrödinger Equation by adopting the Feynman path integral approach over the Levy flights based on non-Gaussian Levy distribution. The derivative of fractional order is known as Levy index (LI), $0 < \alpha \leq 2$. An interesting observation to note is at $\alpha = 2$, Levy motion converts into Brownian motion. Later, (Dong & Xu, 2007) and (Guo & Jiang, 2006) further explored another subject with the addition of specific potential fields. Longhi is credited for introducing the application of SFSE in the optical field whereby he realized laser implementation (Longhi, 2015). Since then, it paved the way

for the optical realization of FSE in optics. Afterwards, (Zhang et al., 2015) investigated optical beam with harmonic potential, (Al-Raeei & El-Daher, 2020) with Riemann-Liouville derivative for SFSE with morse potential, (Ali & Maneea, 2023) for applications of SFSE in the realization of an optical soliton with Riesz derivative. Replacing a second-order space derivative in equation (3) with a space derivative of order α whilst still retaining the first-order time derivative, gives one-dimensional Space FSE (Dong & Xu, 2007)

$$i\hbar \frac{\partial \psi}{\partial t} = -D_\alpha \left(\hbar^2 \frac{\partial^2}{\partial x^2}\right)^{\alpha/2} \psi + V(x)\psi \qquad (4)$$

here, D_α is a parameter dependent on α ($D_\alpha = 1/2\,m$ for $\alpha = 2$, m denotes the mass of a particle), $\left(-\hbar^2 \frac{\partial^2}{\partial x^2}\right)^{\alpha/2}$ is a space fractional operator. Equation (4) can be written in an operator form as

$$i\hbar \frac{\partial \psi}{\partial t} = H_\alpha \psi \qquad (5)$$

where H_α is the fractional Hamiltonian operator with $(1 < \alpha \leqslant 2)$ given as

$$H_\alpha = D_\alpha \left(-\hbar^2 \frac{\partial^2}{\partial x^2}\right)^{\alpha/2} + V(x). \qquad (6)$$

here, $\left(-\hbar^2 \frac{\partial^2}{\partial x^2}\right)^{\alpha/2}$ is the quantum Riesz fractional operator. Based on the methods discussed by Longhi and assuming $\hbar = 1$, equation (4) can be written as

$$i \frac{\partial \psi}{\partial z} = \left[D_\alpha \left(-\frac{\partial^2}{\partial x^2}\right)^{\alpha/2} + V(x)\right] \psi \qquad (7)$$

where z is the propagation distance, α is the fractional order known as LI $(1 < \alpha \leqslant 2)$, the kinetic term in the Hamiltonian, $\left(-\frac{\partial^2}{\partial x^2}\right)^{\alpha/2}$ is represented by the quantum Riesz fractional derivative of the order α defined by

$$\left(-\frac{\partial^2}{\partial x^2}\right)^{\alpha/2}\psi = \frac{1}{2\pi}\int_{-\infty}^{+\infty}dpe^{ipx}|p|^{\alpha}\int_{-\infty}^{+\infty}e^{-ipx}\psi dx. \tag{8}$$

2.2 Fractional Schrödinger Equation in the temporal domain

Another linear FSE is the Time-dependent Fractional Schrödinger Equation (TFSE) or FSE in the temporal domain introduced by (Naber, 2004) defined by Caputo fractional derivatives. Commonly used fractional derivatives for converting integer order derivates to non-integer order derivates in fractional partial differential equations besides Caputo are Riemann-Liouville fractional derivatives and Riesz fractional derivatives (Oldham & Spanier, 1974; Podlubny, 1999). Naber used fractional diffusion equation analogy to derive the TFSE and his work has been followed by (Wang & Jiang, 2007) for space-time FSE in combination with Laskin's derivative.

A recent paper by (Liu et al., 2023) experimentally realized fractional optical medium through fractional GVD in TFSE. Advantages such as spatial profile preservation, easy manipulation of temporal properties, and "fractional phase protector" ensure its realization in current fibre optics along with waveguides and the possibility of including dispersive losses and Kerr nonlinearity effects are strongly indicated. Based on this paper, the FSE in the temporal domain is given for an optical pulse propagating in a complex dispersive material as

$$i\frac{\partial\psi}{\partial z} = \left[\frac{D}{2}\left(-\frac{\partial^2}{\partial\tau^2}\right)^{\alpha/2} - \sum_{k=2,3\ldots}\frac{\beta_k}{k!}\left(i\frac{\partial}{\partial\tau}\right)^k + V(\tau)\right]\psi \tag{9}$$

here, $\psi = \psi(\tau, z)$ is the slowly varying amplitude of the electrical field, z and τ are propagation distance and time derivatives respectively, D is the fractional dispersion coefficient. The first term is the fractional time derivative of the order α, the second term is the regular k^{th} GVD with coefficient β_k and the third term $V(\tau)$, is the potential. So, in equation (9), the fractional derivative is defined in terms of the Riesz fractional operator (Cai & Li, 2019) as

$$\left(-\frac{\partial^2}{\partial\tau^2}\right)^{\alpha/2}\psi = \frac{1}{2\pi}\int_{-\infty}^{+\infty}\int_{-\infty}^{+\infty}d\theta d\omega|\omega|^{\alpha}e^{-i\omega(\theta-\tau)}\psi(\theta) \tag{10}$$

The frequency domain of equation (9) is obtained by applying Fourier Transform which provides a solution as below.

$$\Psi(\omega, z) = \exp\left[-i\left(\frac{D}{2}|\omega|^\alpha - \sum_{k=2,3,...}\frac{\beta_k}{k!}\omega^k\right)z\right]\Psi_{\text{input}}(\omega), \qquad (11)$$

The equation (11) has a frequency domain input wave profile $\Psi_{\text{input}}(\omega)$, which can be manipulated by pulse shapers (Monmayrant et al., 2010; Weiner, 2011). Introducing the fractional phase shift in the frequency domain results in a temporal profile that matches the FSE equation solution.

The experimental setup to realize FSE in the temporal domain to study the pulse dynamic is given by (Liu et al., 2023) in Figure 1(a). The setup is divided into three parts namely:

(1) Initial stage, the input ultrafast pulse is passed through a first hologram to shape the pulse.

(2) Propagation stage, the path emulating Levy waveguide is the second hologram which adds spectral phase shift to the pulse.

(3) Measurement stage, the received pulse's amplitude and phase are obtained by the method of single-shot SSI techniques.
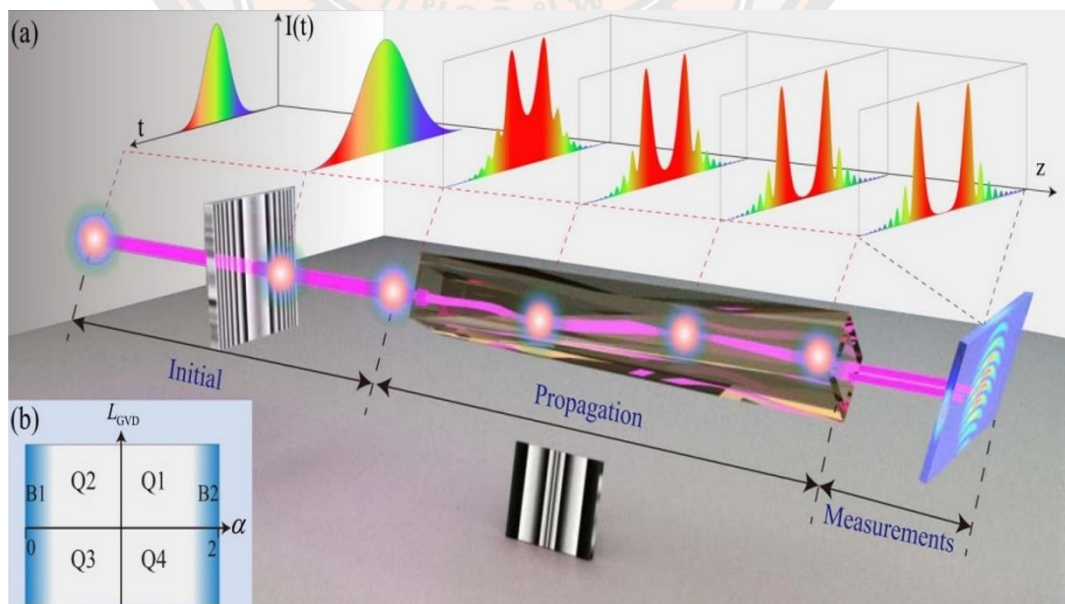
Figure 1 Architectural set-up of FSE in the temporal domain.

The evolution of the pulse depends on both LI and the initial input pulse, $\psi_{\text{input}}(\tau, z = 0)$. At the initial section of the setup, the second-order GVD (β_2) and dispersion length L_{GVD} introduces the phase shift, $\phi_{\text{GVD}} = -\beta_2 * L_{\text{GVD}} * \omega^2/2$, which corresponds to the input pulse in equation (10) where $\Psi_{z=0}(\omega)$ is frequency domain input pulse with Gaussian profile from a laser source.

$$\Psi_{\text{input}}(\tau) = F^{-1}[\Psi_{z=0}(\omega) \cdot \exp(-i\beta_2 L_{\text{GVD}}\omega^2/2)] \tag{12}$$

For the constant value of $\beta_2 = -21 * 10^{-3} ps^2/m$, the effects of L_{GVD} is observed with LI as depicted in Figure 1(b) in four quadrants Q1, Q2, Q3 and Q4. Q1 and Q2 belong to the case with $L_{\text{GVD}} > 0$ whilst Q3 and Q4 with $L_{\text{GVD}} < 0$. As α becomes closer to value 2, the pulse propagation resembles that in the regular dispersive materials whilst it is different for smaller values of α.

2.3 Mathematical analysis of fibre laser

To mathematically depict the transformation of pulses in contemporary fibre lasers, a few physical effects must be considered. Included among these are dispersion effects, fibre nonlinearities, power amplification and losses. The study of such laser systems is more complicated because of the dispersion effects and the nonlinear dynamics of the cavity radiation (Yarutkina et al., 2015). The energy of the soliton is determined by the balance of saturated gain and non-saturated losses in the laser cavity, whereas dispersion and nonlinear factors determine pulse production and form (Turitsyn, 2009; Turitsyn et al., 2012). As a result, dispersion and nonlinear effects can be overlooked when analysing energy dynamics.

The mathematical expression for output energy based on cavity gain/loss parameters is generalized and the Schrödinger equation may accurately represent energy evolution in the gain medium (Haus, 1975; Siegman, 1986).

$$\frac{\partial A}{\partial z} = -\frac{i\beta_2}{2}\frac{\partial^2 A}{\partial t^2} + \frac{\beta_3}{6}\frac{\partial^3 A}{\partial t^3} + i\gamma|A|^2 A + \frac{g_A}{2(1+E/E_{\text{sat}})}A - \frac{\alpha_A}{2}A, \tag{13}$$

The function $A(z, t)$ represents the envelope of the electromagnetic field. The variable z represents the spatial position, while t represents the time. β_2 and β_3 are the dispersion coefficients, and γ is the nonlinear coefficient. The input field is represented by the function $A_{in}(t) = A(z = 0, t)$, where α_A represents the fibre loss coefficient, g_A is the small signal gain, and E_{sat} is the saturation energy.

2.3.1 Application of fractional soliton in fibre laser.

Literature on optical solitons in a fractional medium strongly indicates its application in optical cavities including LASERS. Studies in optical fibre and optical lasers are extensively carried out and it's only natural that the application can be extended to fibre lasers.

This active device is a combination of optical fibre and an amplifier which generates high-power light beams using pump power (Kasai et al., 2017) and supports the simultaneous existence of solitons (Kasai et al., 2018). Initially designed with a traditional optical pulse has now been found to support optical solitons. The key to stable generation and amplification of light beams in a fibre laser is governed by its dynamical properties and controlling those properties is crucial.

The core of the fibre laser is doped with rare earth element which absorbs incoming photons and emits high-power optical beams. These highly precise beams are used in medicines and industries.

2.4 Optical soliton in fractional medium

One-dimensional (1D) Fractional Nonlinear Schrödinger Equation (FNLSE) of optical soliton given by (Malomed, 2021), is

$$i\frac{\partial \psi}{\partial z} = \frac{1}{2}\left(-\frac{\partial^2}{\partial x^2}\right)^{\alpha/2}\psi + V(x)\psi - g|\psi|^2\psi \tag{14}$$

where $\psi = \psi(x, z)$ is the slowly varying amplitude of the optical field, z and x are the propagation distance and transverse coordinates respectively, g is the Kerr nonlinearity coefficient. The fractional derivative with the LI, α is defined, in the form of the Riesz derivative,

$$\left(-\frac{\partial^2}{\partial x^2}\right)^{\alpha/2}\psi = \frac{1}{2\pi}\int_{-\infty}^{+\infty}dp|p|^{\alpha}\int_{-\infty}^{+\infty}d\xi e^{ip(x-\xi)}\psi(\xi) \tag{15}$$

The basic soliton family solution of the equation (15) with propagation constant $-\mu$ is given as

$$\psi(x,z) = U(x)\exp{(-i\mu z)} \tag{16}$$

with real function $U(x)$ satisfying the stationary equation and without potential ($V = 0$).

$$\mu = -\frac{1}{2}\left(\frac{\partial^2}{\partial x^2}\right)^{\alpha/2}U - gU^3 \tag{17}$$

The stationary states are characterized by their energy (N).

$$N = \int_{-\infty}^{+\infty}|U(x)|^2 dx \tag{18}$$

The effect of LI on the profile of solitons after solving equation (16) utilizing the Modified Squared Operator method (MSOM) is given in Figure 2.
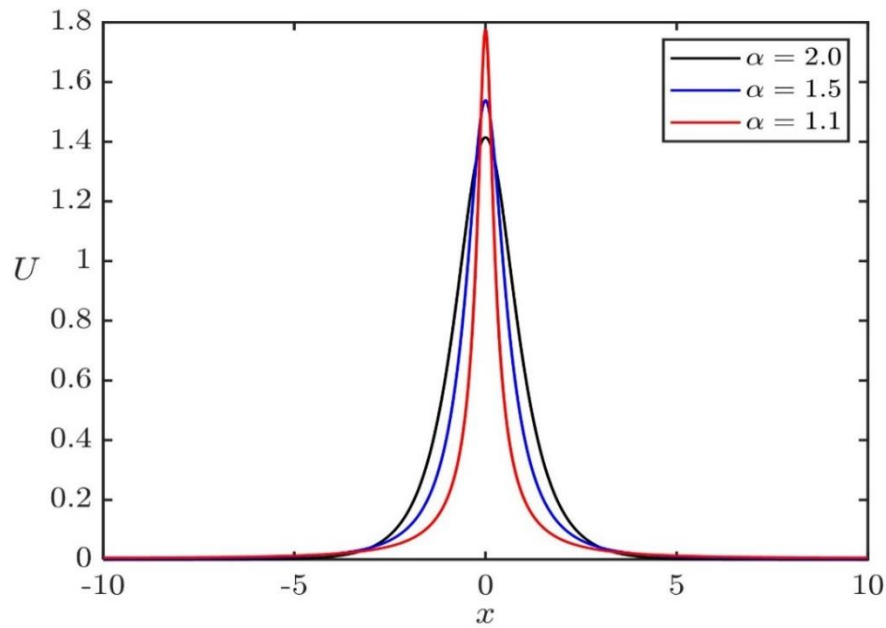
Figure 2 Initial soliton profile for μ =1.

The temporal propagation of these solitons for different values of LI is given below.

(a)

(b)

(c)
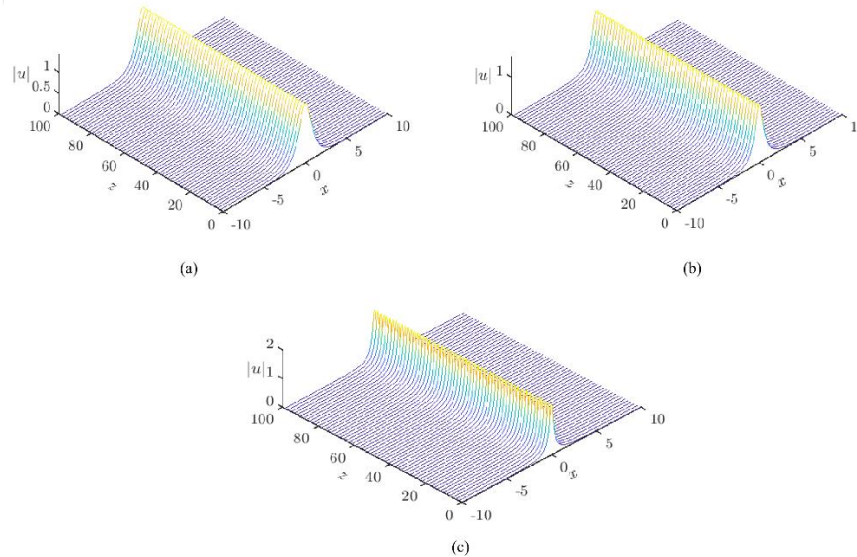
Figure 3 The evolution of stable fractional solitons for α =2 (a); α =1.5 (b) and α =1.1(c)

2.4.1 Collision between soliton in optical fibre.

The transmission of optical information has benefited immensely from WDM techniques with simultaneous transmission of several separate channels over the SMF. Solitons in the WDM system further propelled the capacity of the optical transmission system with its characteristics and stability. A WDM soliton system suffers from collisions among soliton channels as they propagate at proximity. It is observed that, aside from slight temporal and phase shifts experienced by the solitons during collisions, it fully regains its original self after collision.

If the assumption is that the nonlinear effects have a negligible impact on the fibre modes, it may simplify the equation by factoring out the transverse dependence and writing a slowly varying function of time as $E_j(r,t)$ in the form (Agrawal, 2019).

$$E_j(r,t) = F_j(x,y)A_j(z,t)\exp(i\beta_{0j}z) \tag{19}$$

where $F_j(x,y)$ is the transverse distribution of the fibre mode for the jth field ($j = 1,2$), $A_j(z,t)$ is the slowly varying amplitude, and β_{0j} is the corresponding propagation constant. To account for dispersive effects, the frequency-dependent propagation constant $\beta_j(\omega)$ for each wave is expanded with the quadratic term retained. The outcome of this equation for propagation becomes:

$$\frac{\partial A_j}{\partial z} + \beta_{1j}\frac{\partial A_j}{\partial t} + \frac{i\beta_{2j}}{2}\frac{\partial^2 A_j}{\partial t^2} + \frac{\alpha_j}{2}A_j = \frac{in_2\omega_j}{c}\left(f_{jj}|A_j|^2 + 2f_{jk}|A_k|^2\right) \tag{20}$$

here $\beta_{1j} = 1/v_{gj}$, with v_{gj} is the group velocity, β_{2j} is the GVD parameter, α_j is the attenuation coefficient for $k \neq j$. The overlap integral f_{jk} is defined as

$$f_{jk} = \frac{\iint_{-\infty}^{\infty}|F_j(x,y)|^2|F_k(x,y)|^2\,\mathrm{d}x\mathrm{d}y}{\iint_{-\infty}^{\infty}|F_j(x,y)|^2\,\mathrm{d}x\mathrm{d}y\,\iint_{-\infty}^{\infty}|F_k(x,y)|^2\,\mathrm{d}x\mathrm{d}y} \tag{21}$$

The disparities among the overlap integrals can be substantial if the two waves propagate in distinct fibre modes. In single-mode fibres, the values of f_{11}, f_{22} and f_{12}

may vary due to the frequency dependency of $F_j(x, y)$. The disparity is minimal, yet it might be disregarded in practical situations. Therefore, equation (19) can be expressed as a combination of two interconnected nonlinear Schrödinger equations.

$$\frac{\partial A_1}{\partial z} + \frac{1}{v_{g1}}\frac{\partial A_1}{\partial t} + \frac{i\beta_{21}}{2}\frac{\partial^2 A_1}{\partial t^2} + \frac{\alpha_1}{2}A_1 = i\gamma_1(|A_1|^2 + 2|A_2|^2)A_1 \tag{22}$$

$$\frac{\partial A_2}{\partial z} + \frac{1}{v_{g2}}\frac{\partial A_2}{\partial t} + \frac{i\beta_{22}}{2}\frac{\partial^2 A_2}{\partial t^2} + \frac{\alpha_2}{2}A_2 = i\gamma_2(|A_2|^2 + 2|A_1|^2)A_2 \tag{23}$$

where the nonlinear parameter γ_j is defined as

$$\gamma_j = n_2\,\omega_j/(cA_{eff}),\ (j = 1, 2), \tag{24}$$

here A_{eff} is the effective mode area and assumed the same for both the optical waves.

The evolution of the two pulses along the fibre length is therefore governed by equation (22) and equation (23), which also consider the effects of GVD, SPM, XPM, and group velocity mismatch. For simplicity's sake, if fibre losses are left out, these formulae become:

$$\frac{\partial A_1}{\partial z} + \frac{i\beta_{21}}{2}\frac{\partial^2 A_1}{\partial T^2} = i\gamma_1(|A_1|^2 + 2|A_2|^2)A_1 \tag{25}$$

$$\frac{\partial A_2}{\partial z} + d\frac{\partial A_2}{\partial T} + \frac{i\beta_{22}}{2}\frac{\partial^2 A_2}{\partial T^2} = i\gamma_2(|A_2|^2 + 2|A_1|^2)A_2 \tag{26}$$

where

$$T = t - \frac{z}{v_{g1}}, \qquad d = \frac{v_{g1} - v_{g2}}{v_{g1}v_{g2}} \tag{27}$$

here, T is time measured in a reference frame moving with the pulse travelling at the speed v_{g1} and d is a group velocity mismatch between the two pulses.

2.5 Numerical methods for finding soliton solution.

The dynamic nature of numerous physical phenomena is significantly influenced by nonlinearity, including but not limited to nonlinear wave motions, mechanical vibrations, population dynamics, electronic circuits, laser physics, astrophysics, the heartbeat, plasma physics, and chemical reactions in solutions. Nonlinear evolution equations (NLEEs) such as the Korteweg de Vries equation (KdV), the sine Gordon equation and the nonlinear Schrödinger equation (NLSE) are developed to characterize these processes.

A fractional version of NLSE is one such nonlinear equation used for studying the evolution of wave propagation of optical solitons in nonlinear optics. The soliton solutions of this equation are majorly applied in optics and photonics for ultrafast laser pulses and in optical devices for manipulating particles. The investigation of exact or analytical solutions for solitary waves and soliton is crucial for understanding diverse nonlinear processes despite their complexities and extreme difficulty in obtaining them.

Another alternative approach resorted by many researchers is the numerical approach based on approximations which are easier to compute and solve, however are prone to certain errors. Simulating nonlinear fractional dynamics and evolution is carried out using various numerical methods such as finite difference methods and function approximation methods. An interesting classification of numerical methods is iteration methods as the name suggests, the solution is obtained by repeated calculation of the equations with initial approximation and finding the convergence to the desired results. Common iteration methods used for soliton solutions are Newton's methods (Cheung, 1979), Petviashvili method (Petviashvili, 1976), shooting methods (Yang, 2002) and Self-consistency methods however one or the other falls short of giving the desired results due to one or the other reasons.

In 2007, Yang and Lakoba proposed a new iteration method that fulfilled most of the conditions in terms of accuracy, insensitivity to the number of dimensions, time efficiency, and inclusivity of all the solitary waves (Yang & Lakoba, 2007). The squared operator method (SOM) and modified SOM (MSOM) are termed universally convergent iteration methods for solitary waves in general. The SOM is given as

$$\mathbf{u}_{n+1} = \mathbf{u}_n - \left[\mathbf{M}^{-1}\mathbf{L}_1^{\dagger}\mathbf{M}^{-1}\mathbf{L}_0\mathbf{u}\right]_{\mathbf{u}=\mathbf{u}_n}\Delta t. \tag{28}$$

where $\mathbf{L}_0\mathbf{u}$ is a general solitary wave, $\mathbf{u}$ is the vector solitary wave solution, $\mathbf{L}_1$ is the linearized operator of $\mathbf{L}_0\mathbf{u}$ in the case of complex-valued, $\mathbf{M}$ is the real-valued positive definite Hermitian operator which also accelerates the process, Δt is the time step.

SOM when modified further could converge faster than SOM and MSOM is given as

$$\mathbf{u}_{n+1} = \mathbf{u}_n - \left[\mathbf{M}^{-1}\mathbf{L}_1^{\dagger}\mathbf{M}^{-1}\mathbf{L}_0\mathbf{u} - \alpha_n\langle\mathbf{G}_n, \mathbf{L}_1^{\dagger}\mathbf{M}^{-1}\mathbf{L}_0\mathbf{u}\rangle\mathbf{G}_n\right]_{\mathbf{u}=\mathbf{u}_n}\Delta t \tag{29}$$

where,

$$\alpha_n = \frac{1}{\langle\mathbf{M}\mathbf{G}_n,\mathbf{G}_n\rangle} - \frac{1}{\langle\mathbf{L}_1\mathbf{G}_n,\mathbf{M}^{-1}\mathbf{L}_1\mathbf{G}_n\rangle\Delta t} \tag{30}$$

Users can specify the function, $\boldsymbol{G}_n = \boldsymbol{e}_n \equiv \boldsymbol{u}_n - \boldsymbol{u}_{n-1}$.

These iteration methods are verified for various solitary waves including solitons using NLSE and have suggested its applicability in arbitrary dimensions with little change in the programming and easier to implement.

2.6 Numerical simulations using Split Step Fourier method.

In fibre optics, since both the dispersion and nonlinear effects are represented independently in NLSE, a numerical method is crucial for comprehending the nonlinearity such as the split-step Fourier method (SSFM) (Agrawal, 2000). It can be utilized precisely to simulate the propagation of light pulses through an optical fibre as it is easier to implement and considered a stable approach. Taking a wave equation such as NLSE, it is firstly split into linear and nonlinear operators and then solved independently by applying Fourier Transform (FT) and inverse FT (IFT) as given by (Farag et al., 2021)

$$i\frac{\partial\psi}{\partial z} = \left(-\frac{\partial^2}{\partial x^2}\right)\psi - |\psi|^2\psi \tag{31}$$

where, $L = -\frac{\partial^2}{\partial x^2}$ is the linear operator and $N = -|\psi|^2$ is the nonlinear operator. After

solving separately, the final equation looks like

$$\psi(x, z + \Delta z) = F^{-1}\big(\exp{(-i\omega^2\Delta z)} \cdot F(\exp{(i\Delta z|\psi|^2)}\psi)\big) \qquad (32)$$

Similarly, the introduction of the FSE in optical systems launched possibilities for optical controls (Huang et al., 2017). Features of solitons in Kerr medium have been researched (Huang & Dong, 2016), and nonlinear effects as a function of the Lévy index have been studied by (Zhang et al., 2016). The optical soliton propagation based on nonlinear FSE is given by (Ghalandari & Solaimani, 2019)

$$i\frac{\partial\psi}{\partial z} = \left[\frac{1}{2}\left(-\frac{\partial^2}{\partial x^2}\right)^{a/2} - i|\psi|^2 + V(x)\right]\psi \qquad (33)$$

here, ψ is the amplitude, z and x are the propagation distance and transverse coordinate, respectively. Using SSFM, the equation (31) can be written in the form as

$$i\frac{\partial\psi}{\partial z} = (\widehat{D} + \widehat{N})\psi \qquad (34)$$

where $\widehat{D}$ is the linear differential operator and $\widehat{N}$ is the nonlinear operator.

$$\widehat{D} = -\frac{i}{2}\left(-\frac{\partial^2}{\partial x^2}\right)^{\frac{a}{2}} - iV(x) \qquad (35)$$

$$\widehat{N} = i|\psi|^2 \qquad (36)$$

The final equation after FT and IFT looks like

$$\psi(z + h, x) \cong F^{-1}\exp\left[-\left(\frac{i}{2}\right)h|k|^a\right]F\exp\left[-ih(V(x) - i|\psi|^2]\psi \qquad (37)$$

here, h is the short distance considered for the equation, F stands for FT and F^{-1} stands for IFT, k is the wave number in the Fourier domain. By solving the FSE by the SSFM approach, they have shown the effects of LI on the amplitude of the oscillation, dispersion, and the position of the peak intensity. This study can be used as a reference base for many such studies using various solitons in nonlinear FPDEs.

CHAPTER III

METHODOLOGY

3.1 Introduction

This chapter outlines the methodology employed to solve the equation governing the model in fractional and WDM settings by numerical simulation.

3.2 Research approach

For this research, a computational and numerical simulation approach is chosen. The theoretical information related to optical soliton in fractional NLSE and their dynamics in co-propagating when interpreted in terms of simulation work, the understanding and the replication of the work becomes easier for future researchers to perform and verify or modify the work.

Finding exact or analytical solutions is challenging and often difficult to obtain, another simpler and more effective approach is adopting numerical methods to obtain approximate solutions. Therefore, the numerical simulation-based approach is the right choice for this study.

To calculate the absolute error, the comparison of the approximate values to the equivalent values of the known exact answer is performed. As a result, it can be concluded that the employed methods are highly effective, dependable, and straightforward to implement in a series form that converges rapidly to the precise solution, thus demonstrating the methods' benefits.

3.3 Research model

The models are based on the system of coupled fractional NLS equations, which are relevant for fibre optic (fibre lasers) (Liu et al., 2023) are

$$i\frac{\partial u}{\partial z} = \frac{1}{2}\left(-\frac{\partial^2}{\partial \tau^2}\right)^{\alpha/2} u + (|u|^2 + 2|v|^2)u \tag{38}$$

$$i\frac{\partial v}{\partial z} = -ic\frac{\partial v}{\partial \tau} + \frac{1}{2}\left(-\frac{\partial^2}{\partial \tau^2}\right)^{\alpha/2} v + (|v|^2 + 2|u|^2)v \qquad (39)$$

where real u and v are the two different soliton channels or wavelengths, c is the difference of the inverse group velocity between the two waves, and the Levy index α ($1 < \alpha \leq 2$), represents the fractional group-velocity dispersion (GVD).

The fractional derivative is defined as the Riesz derivative, i.e.,

$$\left(-\frac{\partial^2}{\partial \tau^2}\right)^{\alpha/2} u = \frac{1}{2\pi}\int_{-\infty}^{+\infty} d\omega |\omega|^\alpha \int_{-\infty}^{+\infty} d\xi e^{i\omega(t-\tau)} u(t) \qquad (40)$$

The system has three dynamical invariants: two norms(energies):

$$E_u = \int_{-\infty}^{+\infty} |u(\tau)|^2 d\tau, \qquad E_v = \int_{-\infty}^{+\infty} |v(\tau)|^2 d\tau \qquad (41)$$

The total momentum,

$$p = i\int_{-\infty}^{+\infty} \left(u\frac{\partial u^*}{\partial \tau} + v\frac{\partial v^*}{\partial \tau}\right) d\tau \qquad (42)$$

3.3.1 Collisions between solitons

It is well known that equations (38)-(39) admit stable single-component soliton solutions,

$$u(z,t) = \exp(ik_u z)\, U(\tau), v = 0, \qquad (43)$$

$$u = 0, v(z,t) = \exp(ik_v z)V(\tilde{\tau}), \tilde{\tau} \equiv \tau - cz + \tau_0 \qquad (44)$$

where k_u and k_v are positive propagation constants (generally speaking, $k_u \neq k_v$), τ_0 is an initial temporal distance between the two solitons, and functions $U(\tau)$ and $V(\tau)$, which may be assumed real, and satisfy equations.

$$k_u U + \frac{1}{2}\left(-\frac{d^2}{d\tau^2}\right)^{\alpha/2} U + U^3 = 0 \tag{45}$$

$$k_v V + \frac{1}{2}\left(-\frac{d^2}{d\tau^2}\right)^{\alpha/2} V + V^3 = 0 \tag{46}$$

It may be enough to focus on the case of $k_u = k_v \equiv k$, when two equations (45) and (46) are identical. Then, employing scaling, we may set $k \equiv 1$.

We apply the MSOM method to equation (43) with k=1 for various values of LI, starting from the initial condition.

$$u(0,\tau) = a_0 exp\left(-\tau^2\right), \tag{47}$$

$$v(0,\tau) = a_0 exp\left(-(\tau - \tau_0)^2\right), \tag{48}$$

where a_0 is constant, $\tau_0 = 8.0$ is chosen as an optimal value which is neither too large (takes longer time to observe collision) nor too small (collision observed will be too fast) to efficiently observe collision at the optimum separation. In addition, we choose the acceleration operator **M** as

$$\mathbf{M} = \mathbf{M}_u = \mathbf{M}_v = \gamma - \frac{1}{2}\left(-\frac{\partial^2}{\partial\tau^2}\right)^{\alpha/2} \tag{49}$$

The temporal derivatives as well as $\mathbf{M^{-1}}$ are computed by the discrete Fourier transform. The computational domain is $-128 \leq \tau \leq +128$, discretized in each dimension by 2048 grid points. For this scheme, we found that the optimal (or nearly optimal) parameters is $(\gamma, \Delta t) = (3.8, 0.6)$ for MSOM. With these choices of parameters, the error diagrams versus the number of iterations are displayed in Figures 4 and 5. Here the error is defined as the difference between successive iteration functions:

$$e_n = \sqrt{\langle U_n - U_{n-1}, U_n - U_{n-1}\rangle + \langle V_n - V_{n-1}, V_n - V_{n-1}\rangle} \tag{50}$$

We see that all this scheme converges rather quickly at around 100 iterations to reach the error tolerance which is generally accepted and defined at 10^{-10}.
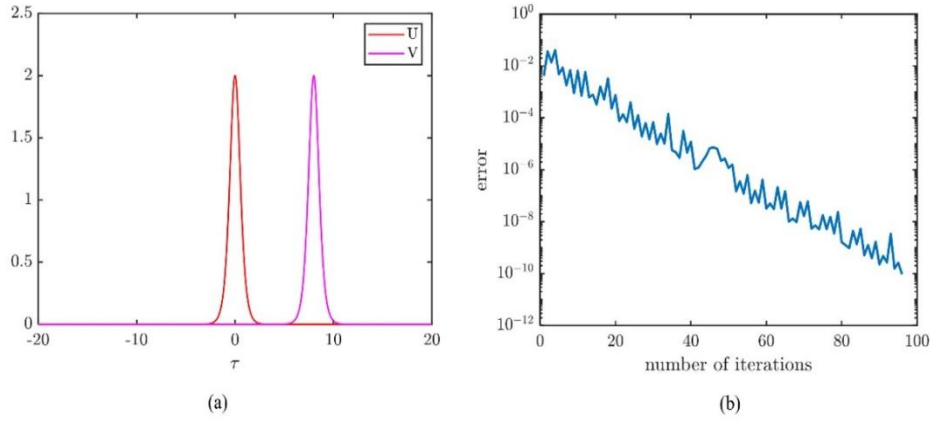
Figure 4 (a) A temporal fractional soliton in equation (44)-(45) and $k = 1$ with $\alpha = 2.0$. (b) error diagrams for MSOM at optimal $(\gamma, \Delta t)$ values (see text).
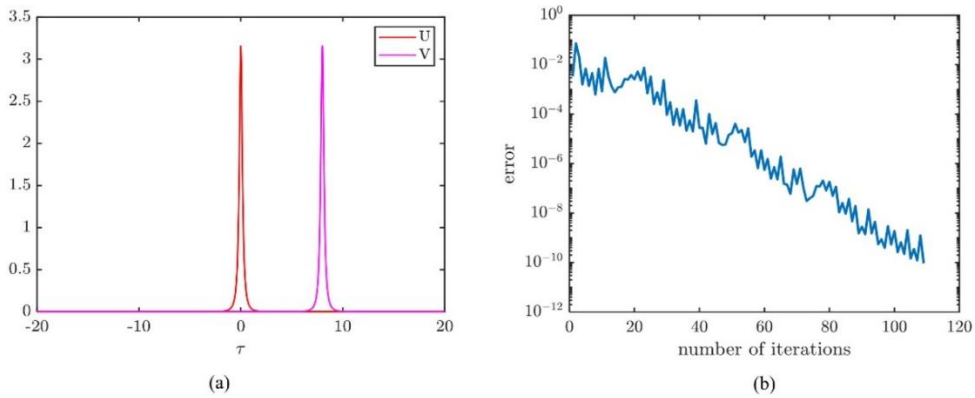
Figure 5 (a) A temporal fractional soliton in equation (44)-(45) and $k = 1$ with $\alpha = 1.1$. (b) error diagrams for MSOM at optimal $(\gamma, \Delta t)$ values (see text).

In the case of the ordinary (non-fractional) GVD, with $\alpha = 2$, the commonly known classical soliton solutions for $k_u = k_v = 1$ are

$$U_{\text{sol}} = \sqrt{2}\,\text{sech}\,(\sqrt{2}\tau), V_{\text{sol}} = \sqrt{2}\,\text{sech}\,(\sqrt{2}\tilde{\tau}) \tag{51}$$

the energy of each one being $E_u = E_v = 2\sqrt{2}$. The numerically found energy for the u and v profiles as shown in Figure 4 is 2.8284, which is equivalent to the value of E_u

and E_v.

To test the stability, the direct simulations (38)-(39) were performed by using the split-step Fourier method with the optimum step size $\Delta z = 0.01$ and window size $T = 128$. Thus, we take its split operators as

$$\widehat{D}_u = \frac{1}{2}\left(-\frac{\partial^2}{\partial \tau^2}\right)^{a/2} \tag{52}$$

$$\widehat{D}_v = \frac{1}{2}\left(-\frac{\partial^2}{\partial \tau^2}\right)^{a/2} \tag{53}$$

$$\widehat{N}_u = (|u|^2 + 2|v|^2) \tag{54}$$

$$\widehat{N}_v = (|v|^2 + 2|u|^2) \tag{55}$$

$$C_v = -ic\frac{\partial v}{\partial \tau} \tag{56}$$

A typical example of the stable temporal fractional solitons with $c = 0$ for $\alpha = 2.0$ is displayed in Figure 6.
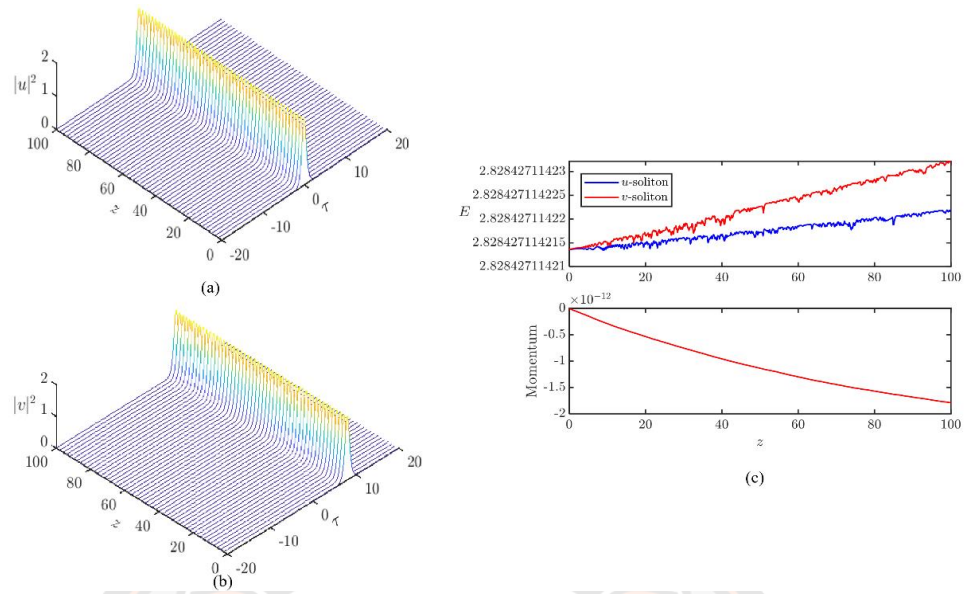
Figure 6 No collision between (a) u-soliton (top left) and (b) v-soliton with $c = 0$ (left bottom) for $\alpha = 2.0$. (c) The energy (right top) and momentum (right bottom) of the system vs. z.
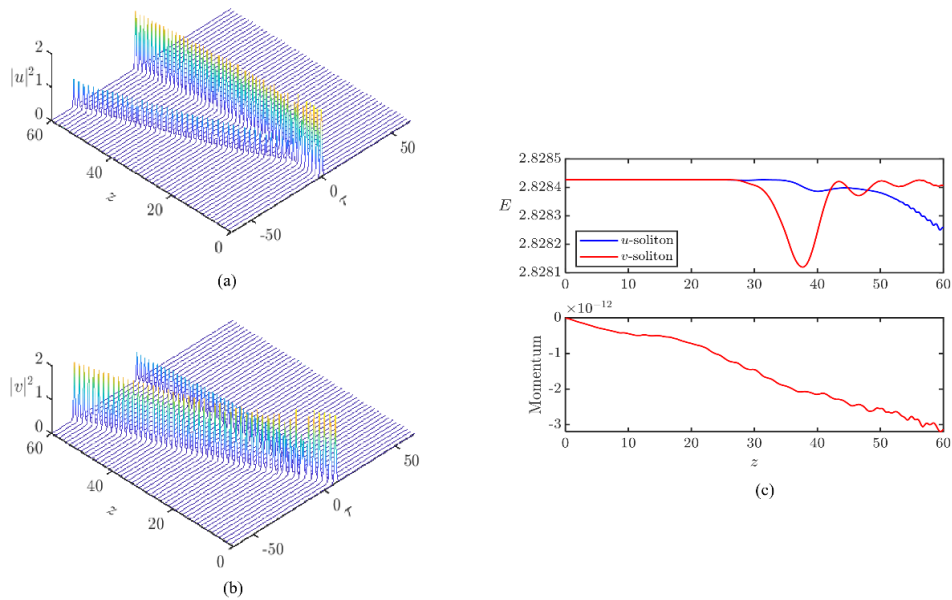
Figure 7 (a) Collision between stationary u-soliton (top left) and (b) v-soliton with $c = -1.0$ (left bottom) for $\alpha = 2.0$. (c) The energy (right top) and momentum (right bottom) of the system vs. z.

One can see from Figure 6 that the u- and v-soliton preserve their shapes over the distance $z = 100$ and do not collide. However, when $c \neq 0$, say $c = -1.0$, u- and v-solitons are splitting into two solitons after collision as shown in Figure 7. In the simulation presented above, the conservation of the dynamical invariants holds with a relative accuracy of $\sim 10^{-6}$. So, in Figures 6 and 7, the variation in the values (y-axis) is negligible and is considered constant and invariant. For u- and v-solitons, the momentum is almost zero and the energy is preserved. This indicates the accuracy of our numerical simulations.

3.3.2 A bound state of two solitons

A stationary bound state of the u- and v-solitons in the system may be looked for in the form of

$$u(z,t) = exp\,(ik_u z)U(\tau), v(z,t) = exp\,(ik_v z)V(\tau), \tag{57}$$

(unlike the above ansatz (43), (44), here functions U and V are not real). As above, we can focus on the case of $k_u = k_v \equiv 1$. Then, the substitution of ansatz (57) in equations (38) and (39) leads to the stationary system:

$$k_u U + \frac{1}{2}\left(-\frac{d^2}{d\tau^2}\right)^{\alpha/2} U + (|U|^2 + 2|V|^2)U = 0 \tag{58}$$

$$k_v V - ic\frac{dV}{d\tau} + \frac{1}{2}\left(-\frac{d^2}{d\tau^2}\right)^{\alpha/2} V + (|V|^2 + 2|U|^2)V = 0 \tag{59}$$

By writing U and V to their real and imaginary components, $U = U_r + iU_i$ and $V = V_r + iV_i$, we get equations for the real functions U_r, U_i, V_r and V_i as

$$L_{ur} \equiv U_r + \frac{1}{2}\left(-\frac{d^2}{d\tau^2}\right)^{\alpha/2} U_r + [U_r^2 + U_i^2 + 2(V_r^2 + V_i^2)]U_r = 0 \tag{60}$$

$$L_{ui} \equiv U_i + \frac{1}{2}\left(-\frac{d^2}{d\tau^2}\right)^{\alpha/2} U_i + [U_r^2 + U_i^2 + 2(V_r^2 + V_i^2)]U_i = 0 \tag{61}$$

$$L_{\text{vr}} \equiv V_{\text{r}} + ic\frac{dV_{\text{i}}}{d\tau} + \frac{1}{2}\left(-\frac{d^2}{d\tau^2}\right)^{\alpha/2} V_{\text{r}} + [2(U_{\text{r}}^2 + U_{\text{i}}^2) + V_{\text{r}}^2 + V_{\text{i}}^2]V_{\text{r}} = 0 \quad (62)$$

$$L_{\text{vi}} \equiv V_{\text{i}} + ic\frac{dV_{\text{r}}}{d\tau} + \frac{1}{2}\left(-\frac{d^2}{d\tau^2}\right)^{\alpha/2} V_{\text{i}} + [2(U_{\text{r}}^2 + U_{\text{i}}^2) + V_{\text{r}}^2 + V_{\text{i}}^2]V_{\text{i}} = 0 \quad (63)$$

Equations (60)-(63) were solved using the Modified Squared Operator Method. For equations (60)-(63), the linearization operator.

$$L_1 = \begin{bmatrix} L_{11} & L_{12} & L_{13} & L_{14} \\ L_{21} & L_{22} & L_{23} & L_{24} \\ L_{31} & L_{32} & L_{33} & L_{34} \\ L_{41} & L_{42} & L_{43} & L_{44} \end{bmatrix}$$

where,

$$L_{11} = \frac{\partial L_{\text{ur}}}{\partial U_{\text{r}}} \equiv k + \frac{1}{2}\left(-\frac{d^2}{d\tau^2}\right)^{\alpha/2} + 3U_{\text{r}}^2 + U_{\text{i}}^2 + 2(V_{\text{r}}^2 + V_{\text{i}}^2)$$

$$L_{12} = \frac{\partial L_{\text{ur}}}{\partial U_{\text{i}}} \equiv 2U_{\text{i}}U_{\text{r}}$$

$$L_{13} = \frac{\partial L_{\text{ur}}}{\partial V_{\text{r}}} \equiv 4V_{\text{r}}U_{\text{r}}$$

$$L_{14} = \frac{\partial L_{\text{ur}}}{\partial V_{\text{I}}} \equiv 4V_{\text{i}}U_{\text{r}}$$

$$L_{21} = \frac{\partial L_{\text{ui}}}{\partial U_{\text{r}}} \equiv 2U_{\text{r}}U_{\text{I}}$$

$$L_{22} = \frac{\partial L_{\text{ui}}}{\partial U_{\text{i}}} \equiv k + \frac{1}{2}\left(-\frac{d^2}{d\tau^2}\right)^{\alpha/2} + U_{\text{r}}^2 + 3U_{\text{i}}^2 + 2(V_{\text{r}}^2 + V_{\text{i}}^2)$$

$$L_{23} = \frac{\partial L_{\text{ui}}}{\partial V_{\text{i}}} \equiv 4V_{\text{r}}U_{\text{i}}$$

$$L_{24} = \frac{\partial L_{\text{ui}}}{\partial V_{\text{i}}} \equiv 4V_{\text{i}}U_{\text{i}}$$

$$L_{31} = \frac{\partial L_{\text{vr}}}{\partial U_{\text{r}}} \equiv 4U_{\text{r}}V_{\text{r}}$$

$$L_{32} = \frac{\partial L_{\text{vr}}}{\partial U_{\text{i}}} \equiv 4U_{\text{i}}V_{\text{r}}$$

$$L_{33} = \frac{\partial L_{\text{vr}}}{\partial V_{\text{i}}} \equiv k + \frac{1}{2}\left(-\frac{d^2}{d\tau^2}\right)^{\alpha/2} + 2(U_{\text{r}}^2 + U_{\text{i}}^2) + 3V_{\text{r}}^2 + V_{\text{i}}^2$$

$$L_{34} = \frac{\partial L_{\text{vr}}}{\partial V_{\text{i}}} \equiv c\frac{d}{d\tau} + 2V_{\text{i}}V_{\text{r}}$$

$$L_{41} = \frac{\partial L_{\text{vi}}}{\partial U_{\text{r}}} \equiv 4U_r V_i$$

$$L_{42} = \frac{\partial L_{\mathrm{vi}}}{\partial U_{\mathrm{i}}} \equiv 4U_i V_i$$

$$L_{43} = \frac{\partial L_{\mathrm{vi}}}{\partial V_{\mathrm{i}}} \equiv 2V_r V_i - c\frac{d}{d\tau}$$

$$L_{44} = \frac{\partial L_{\mathrm{vi}}}{\partial V_{\mathrm{i}}} \equiv k + \frac{1}{2}\left(-\frac{d^2}{d\tau^2}\right)^{\alpha/2} + 2(U_{\mathrm{r}}^2 + U_{\mathrm{i}}^2) + V_{\mathrm{r}}^2 + 3V_{\mathrm{i}}^2$$

The Hermitian of L_1 is the transpose of L_1 and it is given by

$$L_1{}^T = \begin{bmatrix} L_{11} & L_{21} & L_{31} & L_{41} \\ L_{12} & L_{22} & L_{32} & L_{42} \\ L_{13} & L_{23} & L_{33} & L_{43} \\ L_{14} & L_{24} & L_{34} & L_{44} \end{bmatrix}$$

The acceleration operator **M** is taken as equation (48)

$$\mathbf{M} = \mathbf{M}_u = \mathbf{M}_v = \boldsymbol{\gamma} - \frac{1}{2}\left(-\frac{\partial^2}{\partial\tau^2}\right)^{\alpha/2} \tag{64}$$

As the initial condition, we take.

$$U_{\mathrm{r}0} = a_0 exp\left(-(\tau)^2\right), \tag{65}$$

$$U_{\mathrm{i}0} = a_0 exp\left(-(\tau)^2\right), \tag{66}$$

$$V_{\mathrm{r}0} = a_0 exp\left(-(\tau)^2\right), \tag{67}$$

$$V_{\mathrm{i}0} = a_0 exp\left(-(\tau)^2\right)\sin(\tau). \tag{68}$$

where τ_0 is the initial position of the solitons and a_0 is a constant.

In the same case of $\alpha = 2$ but $c = 0$, the obvious solution of equations (58) and (59) is the two-component soliton,

$$u = v = \sqrt{\frac{2}{3}} e^{iz} \mathrm{sech}\left(\sqrt{2}\tau\right) \tag{69}$$

with energies of its components $E_u = E_v = 2\sqrt{2}/3$. In this case, we found simultaneously the numerical energy for u and v, which corresponds to 0.9428, is the same as the analytical one.

In the appendix, the simple MATLAB code for calculating the bound state of two solitons is displayed.

CHAPTER IV

SIMULATION RESULTS

4.1 Introduction

This chapter presents the graphical results of the numerical simulation performed for two cases and the summary of each case is generated.

4.2 Collisions between solitons

In this study, we consider the combined u-soliton and v-soliton as a single-component soliton. To investigate the collisional effects between these two constituents, the u-soliton is designated as the stationary soliton positioned at $\tau = 0$. The v-soliton, characterized by a velocity c, is initially located at $\tau = 8$ and propagates towards the u-soliton.

The collision is observed at $z \approx \tau_0 / c$ where $\tau_0 = 8.0$, the separation between u-soliton and v-soliton. The outcome of the collision is yet to be determined at various values of c. Two control parameters identified are FGVD 'α' and GVD mismatch velocity c.

The reference is $\alpha = 2$, which is the standard non-fractional GVD, and all the results obtained for fractional GVD $1 < \alpha \leq 2$ are compared with standard non-fractional GVD. Firstly, the values of α are fixed and c is varied and the effects of collisions are observed such as elastic, inelastic, quasi-elastic, splitting or merging.

4.2.1 Case I: when α = 2.

In the case of non-fractionality, the LI value is $\alpha = 2$ and when $c = 0$, the system has independent u- and v-solitons propagating separately on its path without ever crossing each other.

The solutions to equations (45) and (46) for u-soliton and v-soliton are found utilizing MSOM. The u-solution for the propagation constant $k_u = k_v = 1$ has the energy

$$E = \int_{-\infty}^{+\infty} |u|^2 \, d\tau = 2.8284 \text{ or } 141.42 \text{ pJ and}$$

the width of the solitons $\tau_{FWHM} = 1.2465$. As the initial condition, we take,

$$u(0, \tau) = \exp\left(-\tau^2\right)$$
$$v(0, \tau) = \exp\left(-(\tau - \tau_0)^2\right) \tag{70}$$

The direct simulation of equations (38) and (39) is performed by employing the Split-Step Fourier method. The τ-interval is taken to be [128, 128], discretized by 4096 grid points, and the discrete Fourier transform is used to calculate $(-\partial^2 / \partial \tau^2)^{\alpha/2}$.

When the velocity $c < 1$ such as $c = $ -1, both u- and v-solitons demonstrate splitting into two solitons after collisions as displayed in Figure 8. The formation of a pair of two-component solitons indicates an inelastic outcome, with unequal energies of the components. The emerging compound solitons keep approximately the same rapidities (0 or c) that their dominant components had before the collision. For $c > 1$ such as $c = $ -2, a collision between solitons is nearly elastic for $c = $ -2 as seen in Figure 9.

The figure displays both the power profiles of the u- and v-components of the emerging compound solitons and the profile of the frequency chirp,

$$C \equiv -\partial^2 \phi / \partial \tau^2 \tag{71}$$

for these components (ϕ is phase, in each case). A conspicuous chirp is observed only in decaying tails of the emerging solitons, not in their main bodies. The compound solitons keep approximately the same rapidities (0 or c) that their dominant components had before the collision.

Figure 8 (a) Collisions between u-soliton (left top) and v-soliton (left bottom) at c = -1 for α = 2. (b) The top panel presents the initial locations of both the solitons with dotted lines and final location at the end of the propagation distance with solid lines. The middle panels: $|u|^2$ (blue solid lines) and the frequency chirp defined as per equation (71) (black dashed lines), as functions of τ, in the u-component of the two compound solitons generated by the collision, in the final state, at z = 60. The bottom panels: $|v|^2$ (red solid lines) and the frequency chirp (black dashed lines) for the v-component of the same solitons. (c) The energy (top) and the momentum (bottom).

Figure 9 (a) Collisions between _u_-soliton (left top) and _v_-soliton (left bottom) at _c_ = -2 for α = 2. (b) The top panel presents the initial locations of both the solitons with dotted lines and final location at the end of the propagation distance with solid lines. The bottom left panel: |_v_|² (the red solid line) and frequency chirp _C_(τ) (the black dashed line), as functions of τ, in the right soliton in its final state, at = 30. The bottom right panel: |_u_|² (the blue solid line) and _C_(τ) (black dashed line) for the left soliton at _z_ = 30. (c) The energy (top) and the momentum (bottom).

4.2.2 Case II: when α = 1.5.

In this case, a moderate degree of fractionality corresponds to the LI value of α = 1.5. For this fixed LI, when _c_ = -0.3, the outcome after the collision is splitting both the solitons into two unequal components as displayed in Figure 10. The rapidities of the emerging components are the same as the dominant components. When _c_ = -0.5, _u_-soliton and _v_-soliton merge into one soliton and form a breather-like structure along the _v_-soliton path, see Figure 11. When v-soliton with _c_ = -0.6 collides with stationary _u_-soliton, the outcome is quasi-elastic meaning elastic splitting of the

components into unequal components which is different from the previous velocity, see Figure 12. Similarly, collisions at c = -1 also gives an increasing degree of elastic outcomes as seen in Figure 13.

Figure 10 (a) Collisions between u-soliton (left top) and v-soliton (left bottom) at c = -0.3 for α = 1.5. (b) The top panel presents the initial locations of both the solitons with dotted lines and final location at the end of the propagation distance with solid lines. The middle panels: $|u|^2$ (blue solid lines) and frequency chirp $C(\tau)$ (black dashed lines) as a function of τ, for the compound solitons in the final state, at z = 100. The bottom panels: $|v|^2$ (red solid lines) and $C(\tau)$ (black dashed lines) as functions of τ for the solitons at z = 100. (c) The energy (top) and the momentum (bottom).
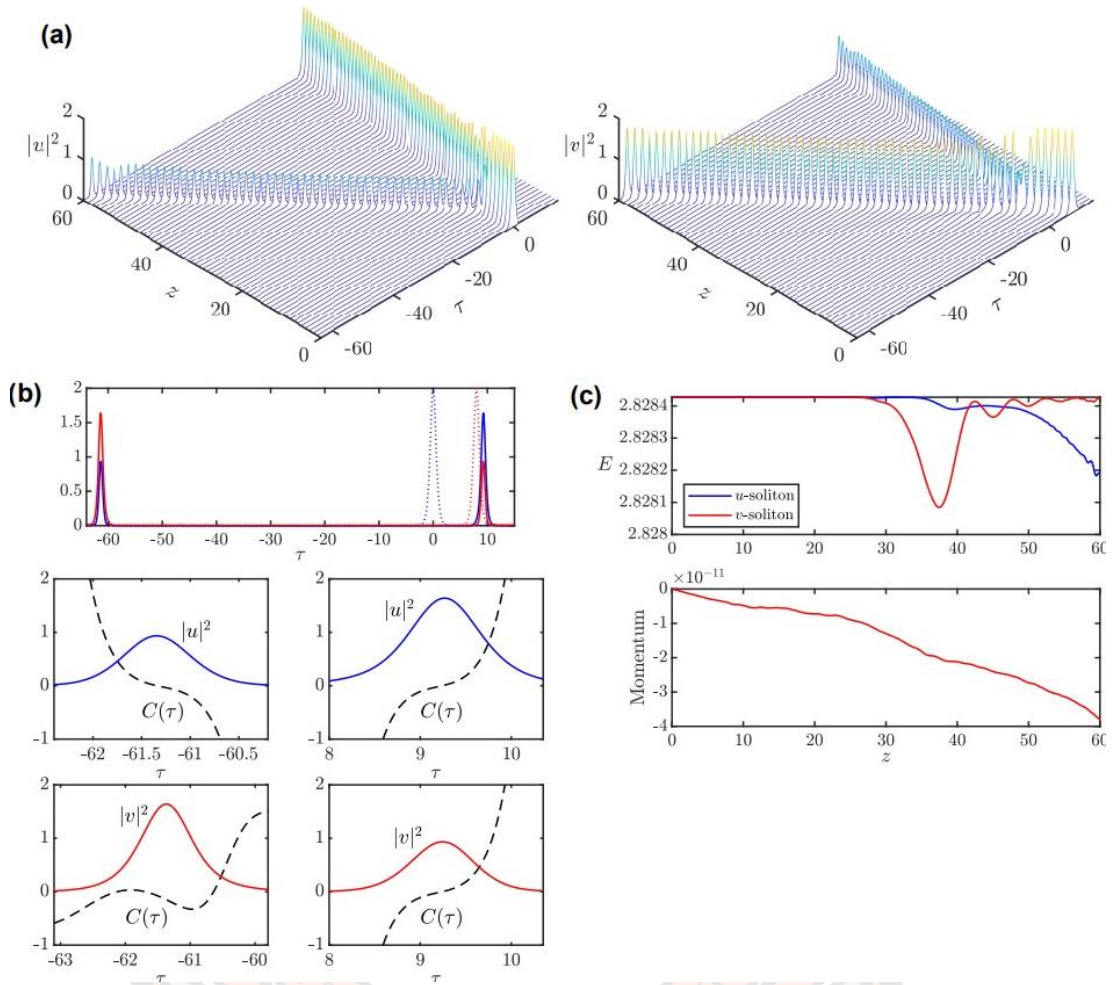
**Figure 11 (a) Collisions between *u*-soliton (left top) and *v*-soliton (left bottom) at
c = -0.5 for α = 1.5. (b) The top panel presents the initial locations of both the
solitons with dotted lines and final location at the end of the propagation distance
with solid lines. The bottom left panel: |*u*|² (blue solid lines) and the frequency
chirp *C*(τ) (black dashed lines) as a function of τ. The bottom right panel: |*v*|²
(red solid lines) and *C*(τ) (black dashed lines) as a function of τ for solitons in the
final state, at *z* = 100. (c) The energy (top) and the momentum (bottom).**
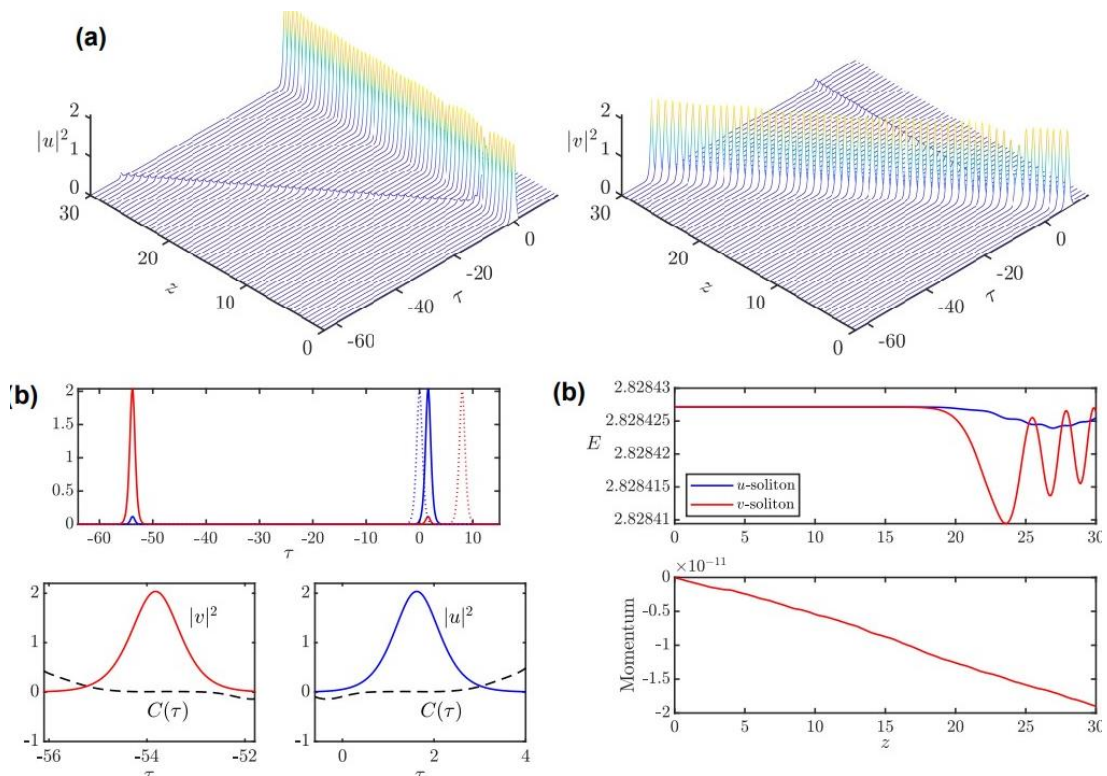
Figure 12 (a) Collisions between *u*-soliton (left top) and *v*-soliton (left bottom) at
c = -0.6 for α = 1.5. (b) The top panel presents the initial locations of both the
solitons with dotted lines and final location at the end of the propagation distance
with solid lines. The middle panels:$|u|^2$ (blue solid lines) and the frequency chirp
$C(\tau)$ (black dashed lines) as functions of τ, in the final state at z = 80. The bottom
panels: $|v|^2$ (red solid lines) and $C(\tau)$ (black dashed lines) as functions of τ for the
solitons at z = 80. (c) The energy (top) and the momentum (bottom).

Figure 13 (a) Collisions between *u*-soliton (left top) and *v*-soliton (left bottom) at

c = -1 for α = 1.5. (b) The top panel presents the initial locations of both the

solitons with dotted lines and final location at the end of the propagation distance

with solid lines. The middle panels: $|u|^2$ (blue solid lines) and the frequency chirp

$C(\tau)$ (black dashed lines) as functions of τ. The bottom panels: $|v|^2$ (red solid

lines) and $C(\tau)$ (black dashed lines) as functions of τ for solitons in the final state

at z = 60. (c) The energy (top) and the momentum (bottom).

4.2.3 Case III: when α = 1.2.

In this case, the fractionality is very strong at α = 1.2 and features different collision outcomes, unlike higher values of α. When c = -0.2, the solitons repulse, and the velocity is exchanged between *u*-soliton and *v*-soliton in a way that the initial velocity of *u*-soliton is c = 0 and after the collision its velocity becomes almost like *v*-soliton. As for the *v*-soliton, it drops its velocity after collision. When c = -0.3 and -0.7, the solitons split into two with breather-like intensity profiles as displayed in

Figures 14 and 15. When the velocity c is increased further such as $c = -5$, the collision outcome is completely elastic as shown in Figure 16.
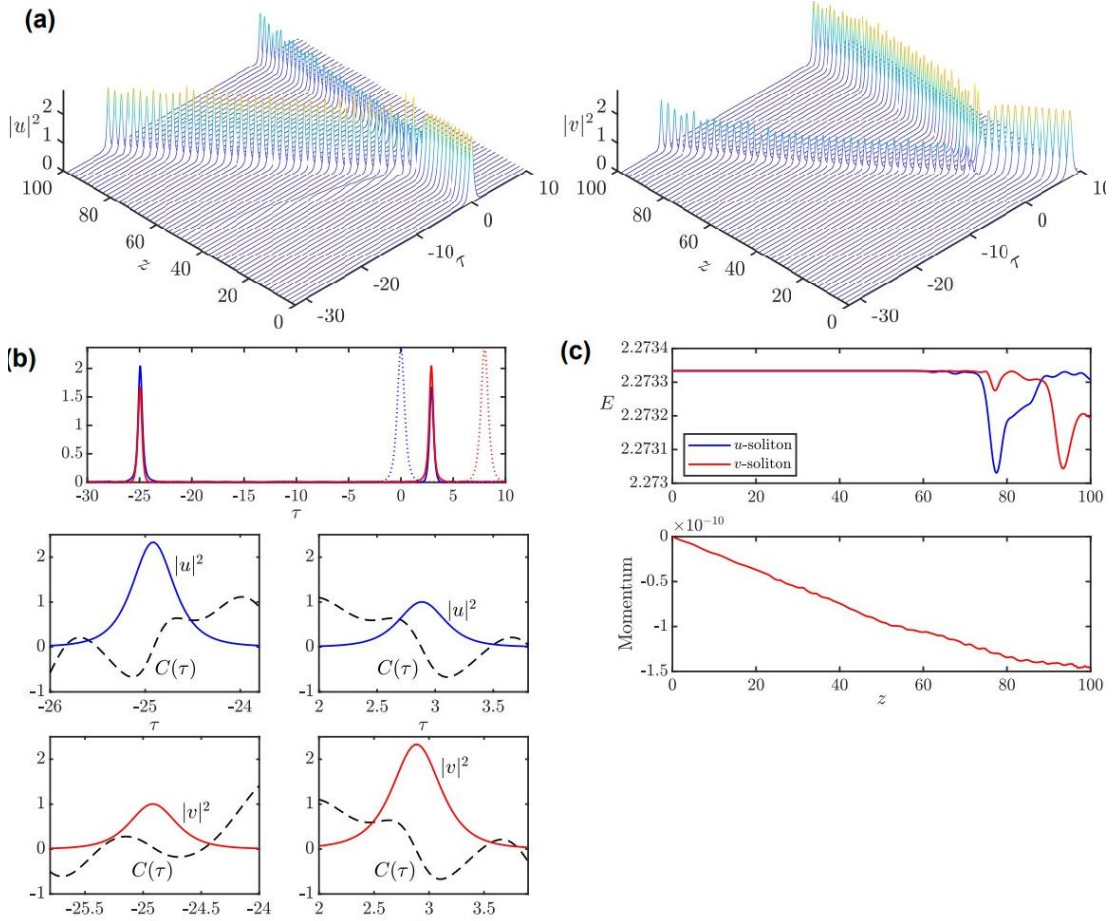

Figure 14(a) Collisions between u-soliton (left top) and v-soliton (left bottom) at c = -0.2 for α = 1.2. (b) The top panel presents the initial locations of both the solitons with dotted lines and final location at the end of the propagation distance with solid lines. The bottom left panel: $|u|^2$ (blue solid lines) and the frequency chirp $C(\tau)$ (black dashed lines) as functions of τ. The bottom right panel: $|v|^2$ (red solid lines) and $C(\tau)$ (black dashed lines), as functions of τ, for the solitons in the final state, at z = 60. (c) The energy (top) and the momentum (bottom).
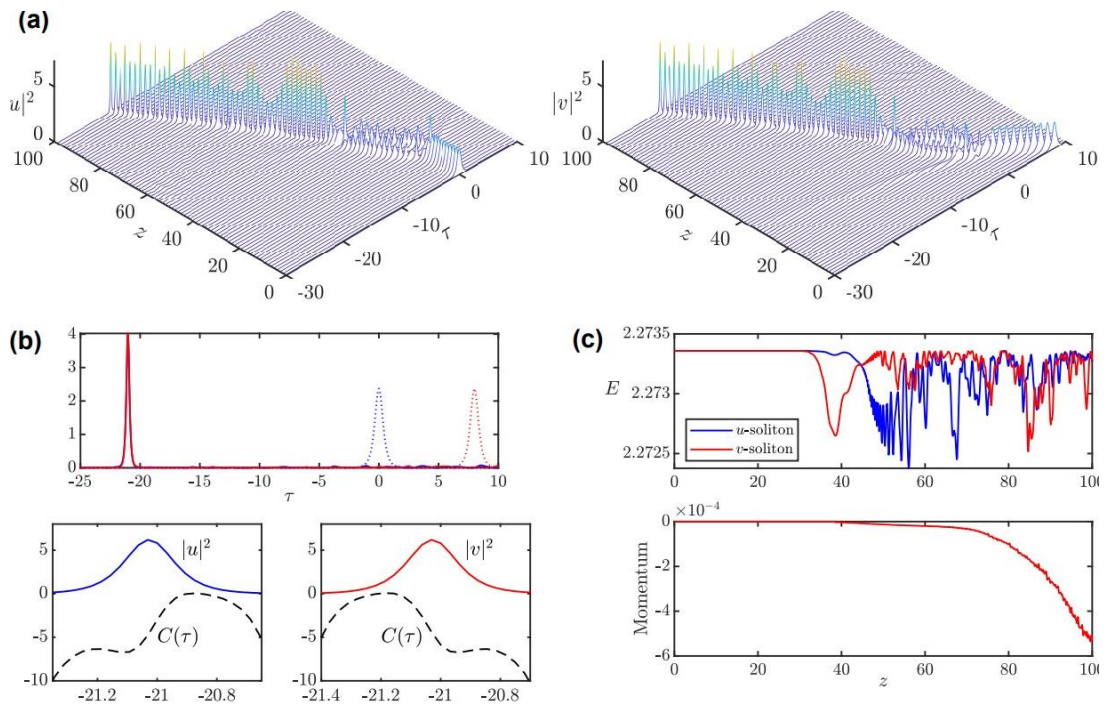
Figure 15 (a) Collisions between *u*-soliton (left top) and *v*-soliton (left bottom) at
c = -0.7 for α = 1.2. (b) The top panel presents the initial locations of both the
solitons with dotted lines and final location at the end of the propagation distance
with solid lines. The middle panel: $|u|^2$ (blue solid lines) and the frequency chirp
$C(\tau)$ (black dashed lines) as functions of τ. The bottom panel: $|v|^2$ (red solid lines)
and $C(\tau)$ (black dashed lines), as functions of τ, for the solitons in the final state,
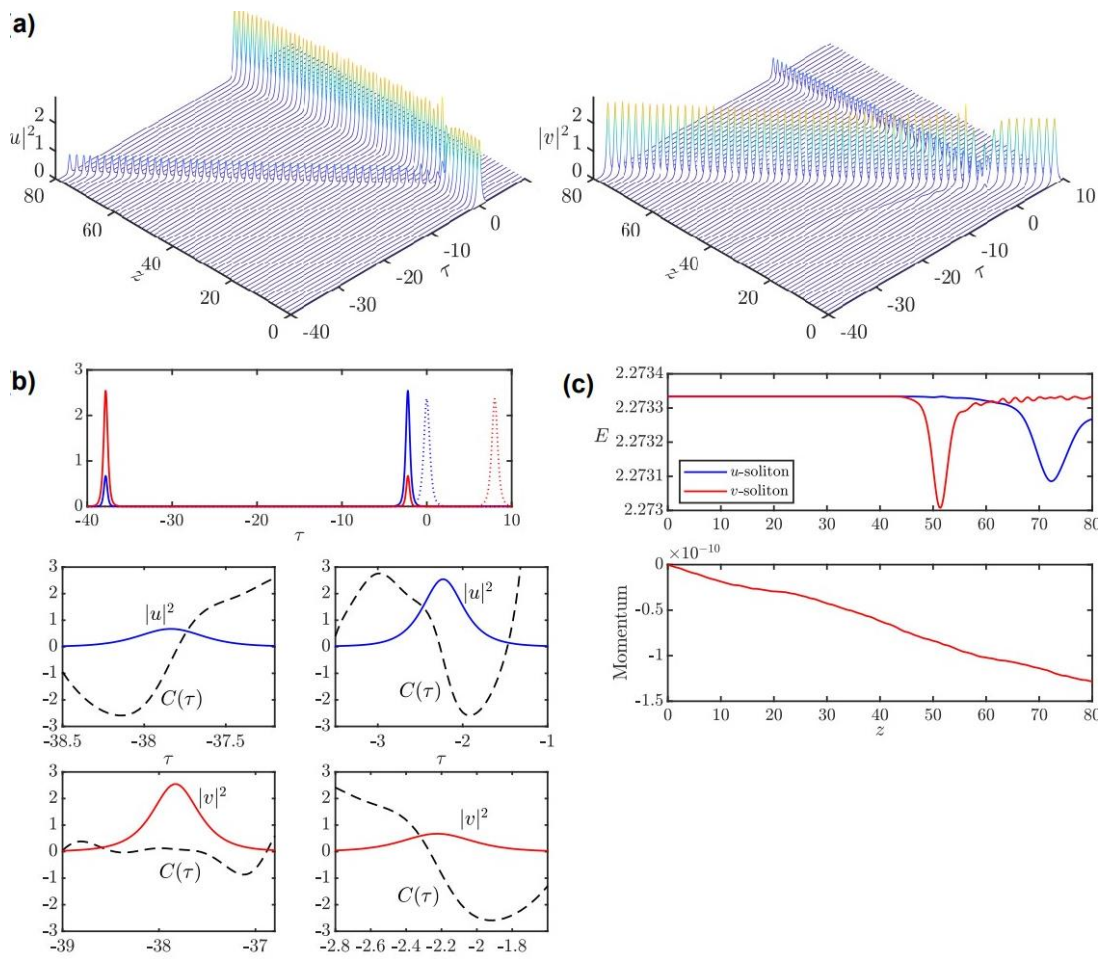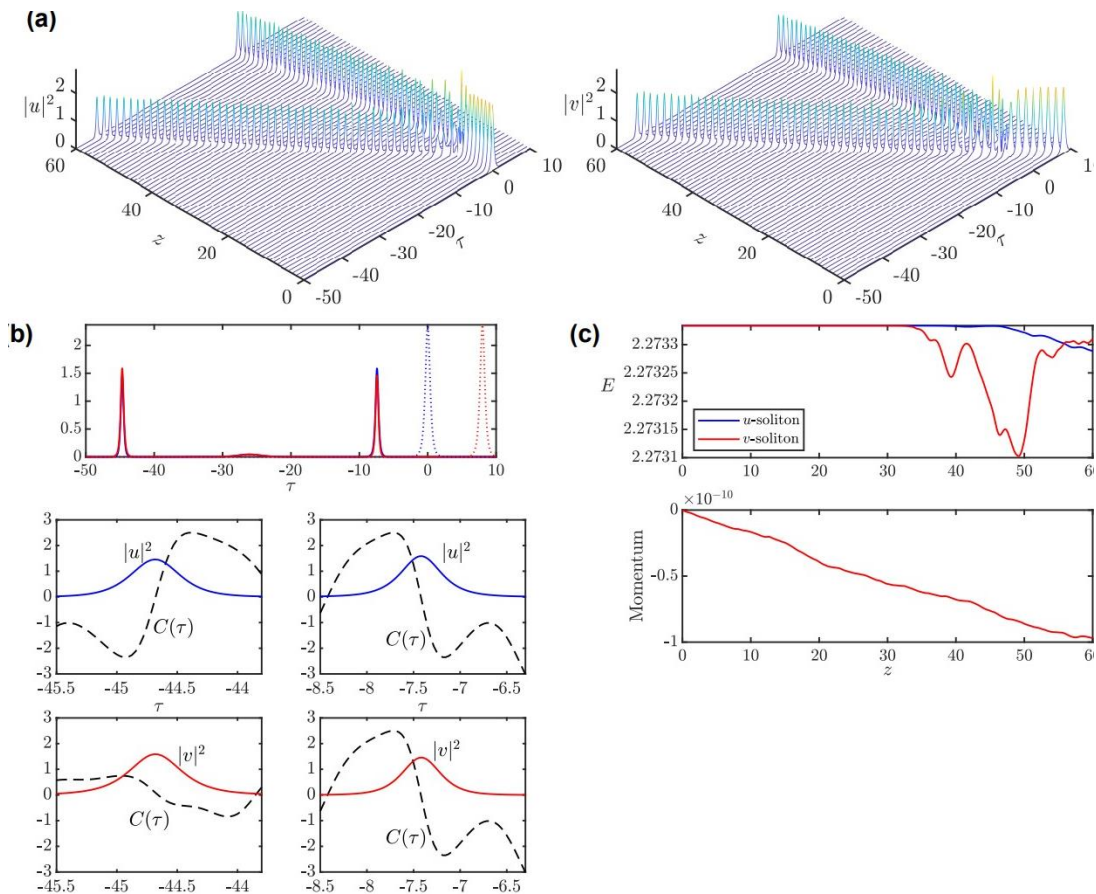**at z = 60. (c) The energy (top) and the momentum (bottom).**
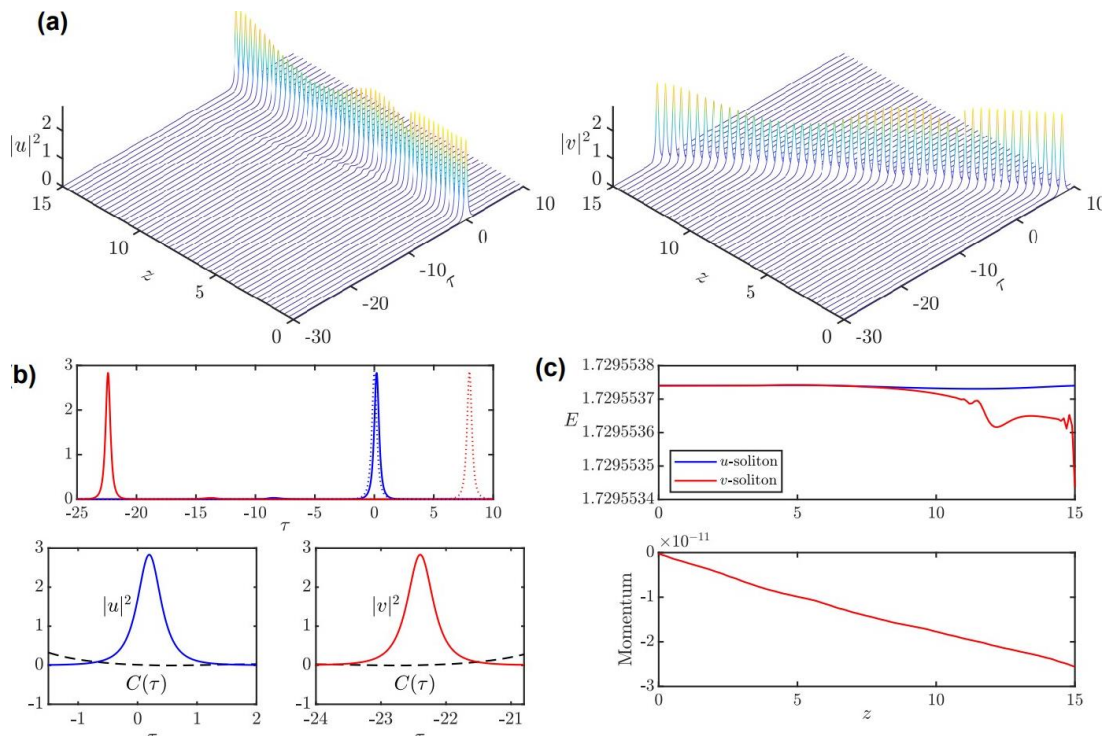
Figure 16 (a) Collisions between *u*-soliton (left) and *v*-soliton (right) at c = -2 for α = 1.2. (b) The top panel presents the initial locations of both the solitons with dotted lines and final location at the end of the propagation distance with solid lines. The bottom left panel: $|u|^2$ (blue solid lines) and the frequency chirp $C(\tau)$ (the black dashed line) as functions of τ. The bottom right panel: $|v|^2$ (the red solid line) and $C(\tau)$ (the black dashed line), as a function of τ, for the solitons in the final states, at z = 15. (c) The energy (top) and the momentum (bottom).

4.2.4 Case IV: when α = 1.1.

In this case, the fractionality is very strong at α = 1.1. When c = -1.1, the solitons split into three components with two strong components with breather-like intensity profile and one with weak intensity plain profile as seen in Figure 17. When the velocity is further increased to c = -1.5, the initial intensity of both the solitons after the collision peaks very high and rapidly drops to a small intensity throughout the distance, see Figure 18. When c = -2, quasi-elastic is the outcome after the collision which results in a periodic breather-like intensity structure as displayed in Figure 19.
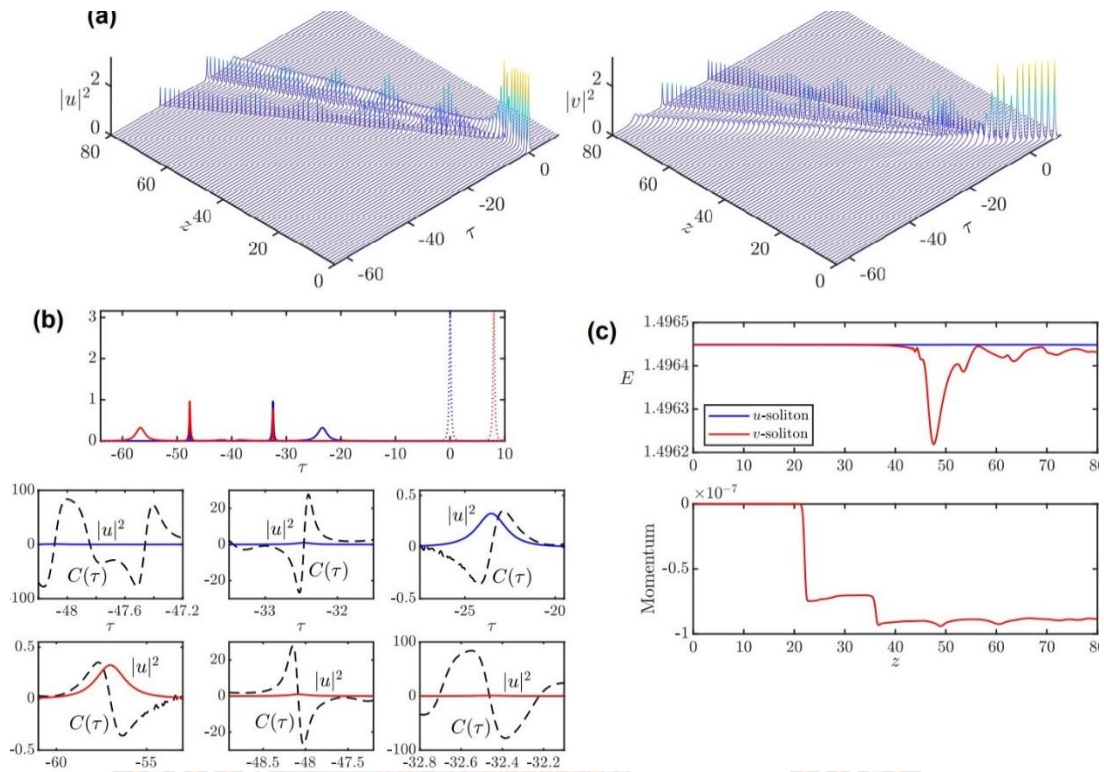
**Figure 17 (a) Collisions between *u*-soliton (left top) and *v*-soliton (left bottom) at
c = -1.1 for α = 1.1. (b) The top panel presents the initial locations of both the
solitons with dotted lines and final location at the end of the propagation distance
with solid lines. The middle panels: |*u*|² (the blue solid line) and the frequency
chirp *C*(τ) (the black dashed line) as functions of τ, for the soliton in the final
state, at *z* = 80. The bottom panels: |*v*|² (the red solid line) and *C*(τ) (the black
dashed line), as functions of τ, for the soliton at *z* = 80. (c) The energy (right) and
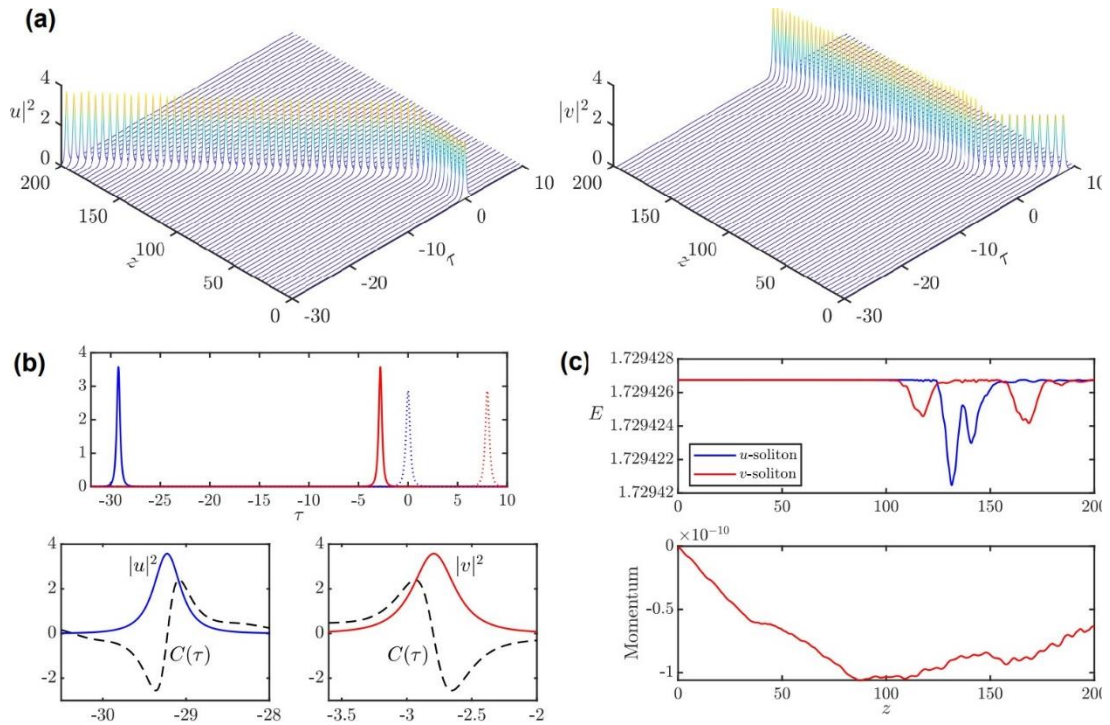the momentum (right).**
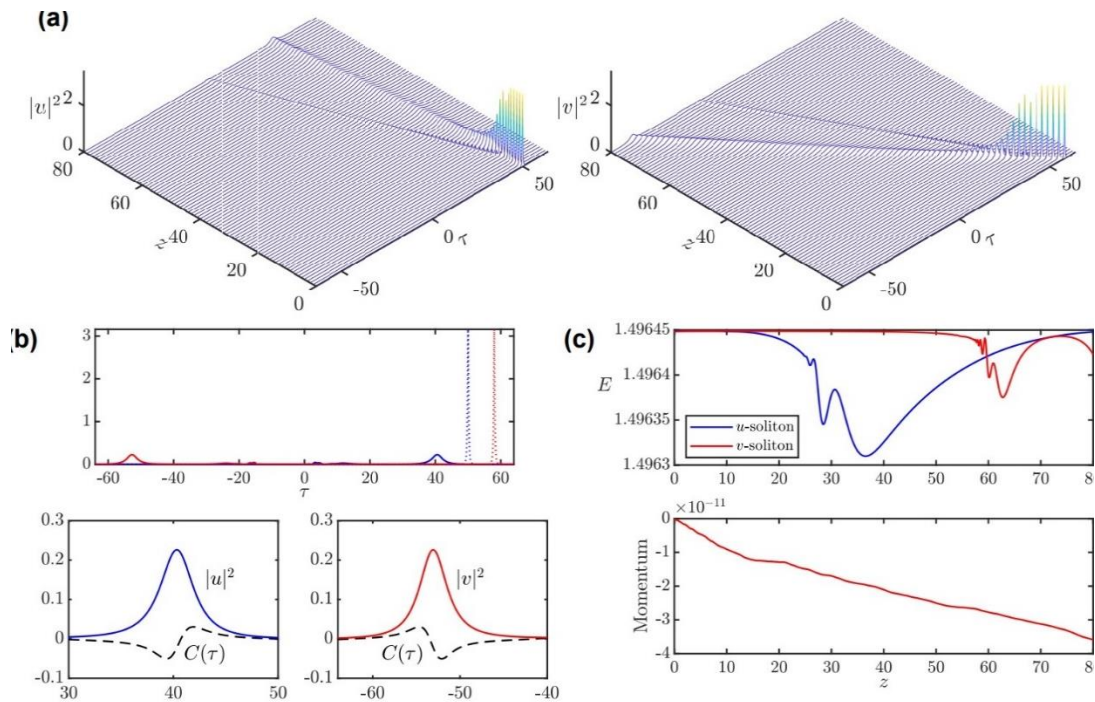
Figure 18 (a) Collisions between u-soliton (left top) and v-soliton (left bottom) at $c = -1.5$ for $\alpha = 1.1$. (b) The top panel presents the initial locations of both the solitons with dotted lines and final location at the end of the propagation distance with solid lines. The bottom left panel: $|u|^2$ (the blue solid line) and the frequency chirp $C(\tau)$ (the black dashed line), as functions of τ in the soliton in the final state, at $z = 80$. The bottom right panel: $|v|^2$ (the red solid line) and $C(\tau)$ (the black dashed line), as a function of τ, for the soliton at $z = 80$. (c) The energy (top) and the momentum (bottom).
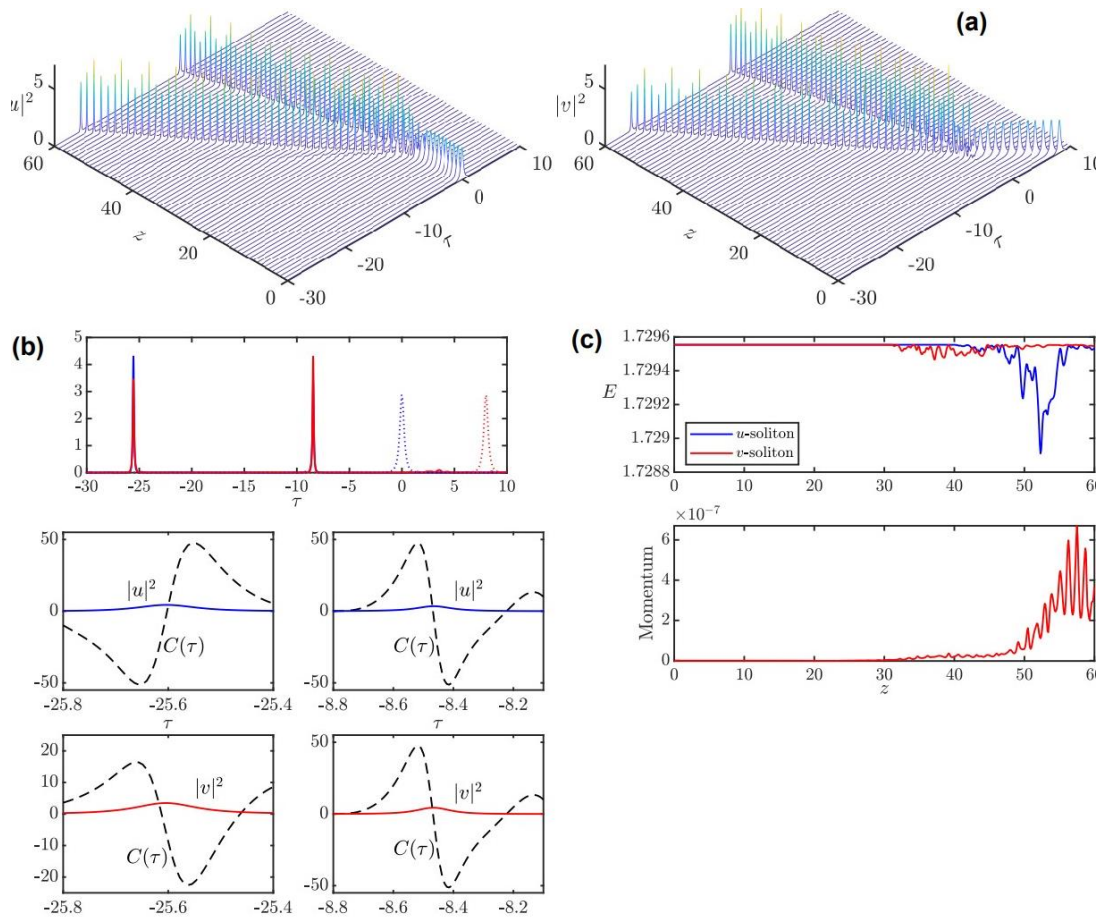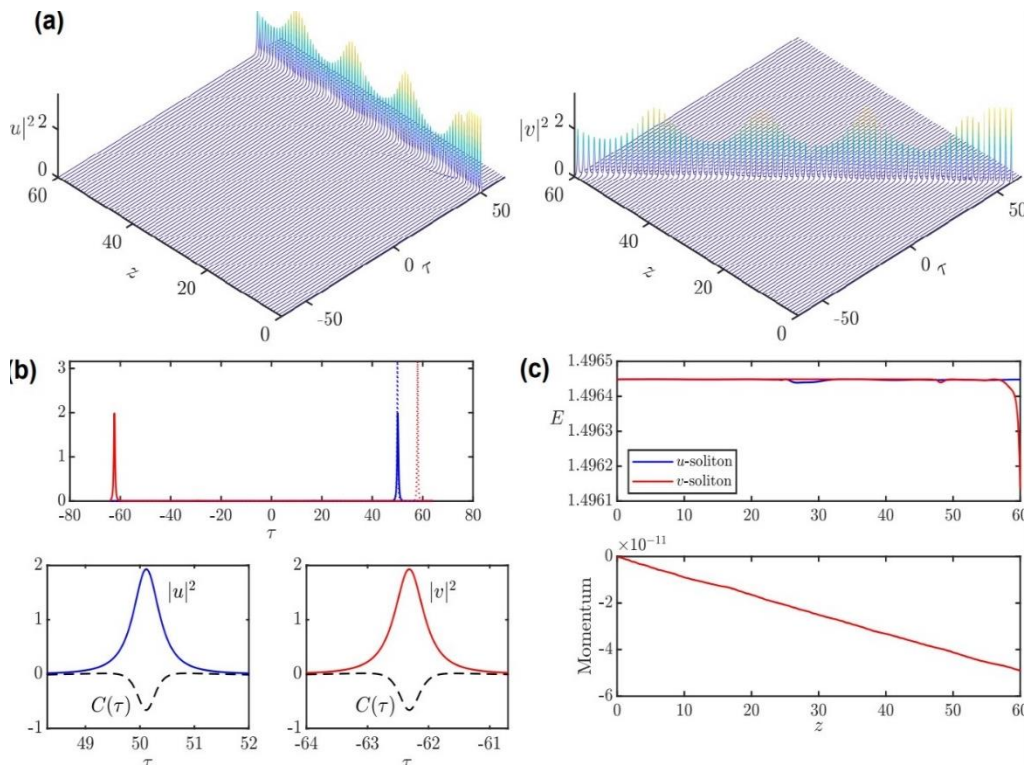
Figure 19 (a) Collisions between u-soliton (left top) and v-soliton (left bottom) at c = -2 for α = 1.1. (b) The top panel presents the initial locations of both the solitons with dotted lines and final location at the end of the propagation distance with solid lines. The bottom left panel: $|u|^2$ (the blue solid line) and the frequency chirp $C(\tau)$ (the black dashed line), as a function of τ, for the soliton in the final state, at z = 60. The bottom right panel: $|v|^2$ (the red solid line) and $C(\tau)$ (the black dashed line), as functions of τ, for the soliton at z = 60. (c) The energy (top) and the momentum (bottom).

## 4.3 Summary of the collisions of two single independent solitons.

Figure 19 below shows the summary of the collisions between u-soliton and v-soliton for various values of α and c. The x-axis displays the LI values between 1 and 2 and correspondingly, the velocity c is on the y-axis.

For lower values of α ($1.1 \leq \alpha \leq 1.3$) with strong fractional GVD, the results of the collision are diverse for lower values of c ($0 \leq c \leq 1.5$) such as repulsion, splitting, and merger followed by splitting and finally for higher velocities ($1.5 \leq c \leq 3$), it enters quasi-elastic and dominates the results.

For moderate values of α (1.4 ≤ α ≤ 1.6) with moderate fractional GVD, the outcomes of the collision for lower values of c are like those of lower values of α however, the majority results in splitting. As the velocity increases from 1.5 to 3, splitting is soon replaced by quasi-elastic.

For higher values of α (1.8 ≤ α ≤ 2) with weak fractional GVD, the main outcome is splitting for all lower and mid-values of c (0 to 2) and above $c = -2$, the outcome is completely elastic.
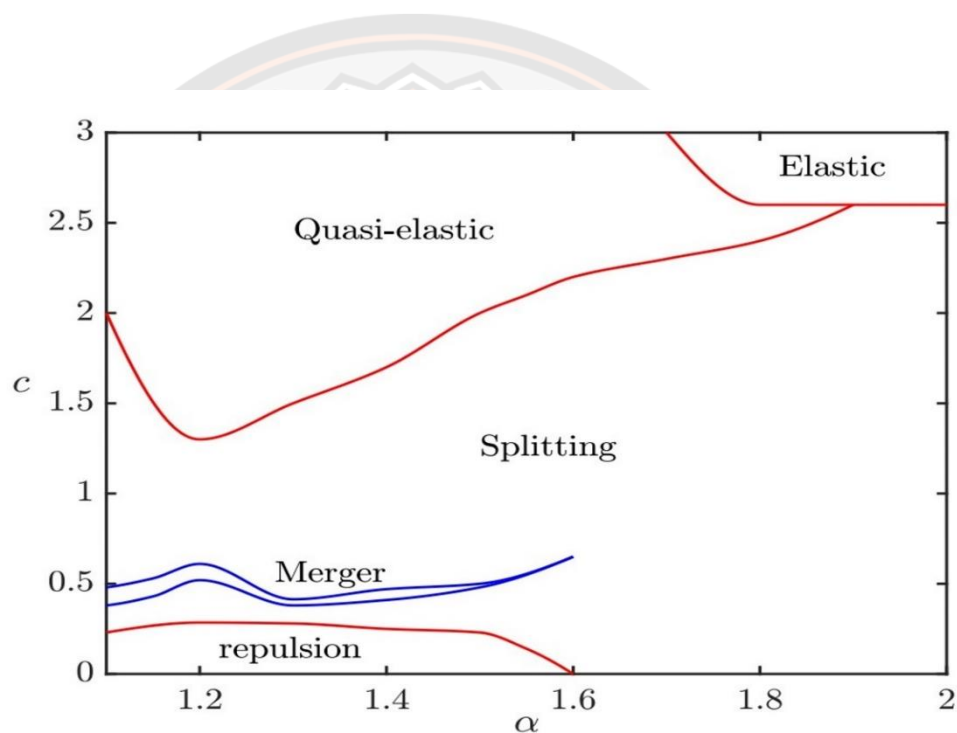
Figure 20 Collision border in the plane (α, c)

4.4 A bound state of two solitons.

Here, the solitons exist simultaneously and are affected by each other's existence and the aim is to observe the outcomes of their collision. Unlike above ansatz (43) and (44), the functions U and V are not real, meaning the complex component must be included which adds complexity to the whole process. Equation (57) when substituted in equations (38) and (39) generates equations (58) and (59) which are in ODE forms and have the presence of XPM coupling.

The two-component solutions of equations (58) and (59) are used as the input for the full system of FNLSEs. As a result, the two-component bound state moves with

deceleration and slightly varying amplitudes, quickly relaxing towards a stable stationary two-component soliton, with a constant rapidity and constant amplitudes of its components at various values of α and c as given in the figures below.
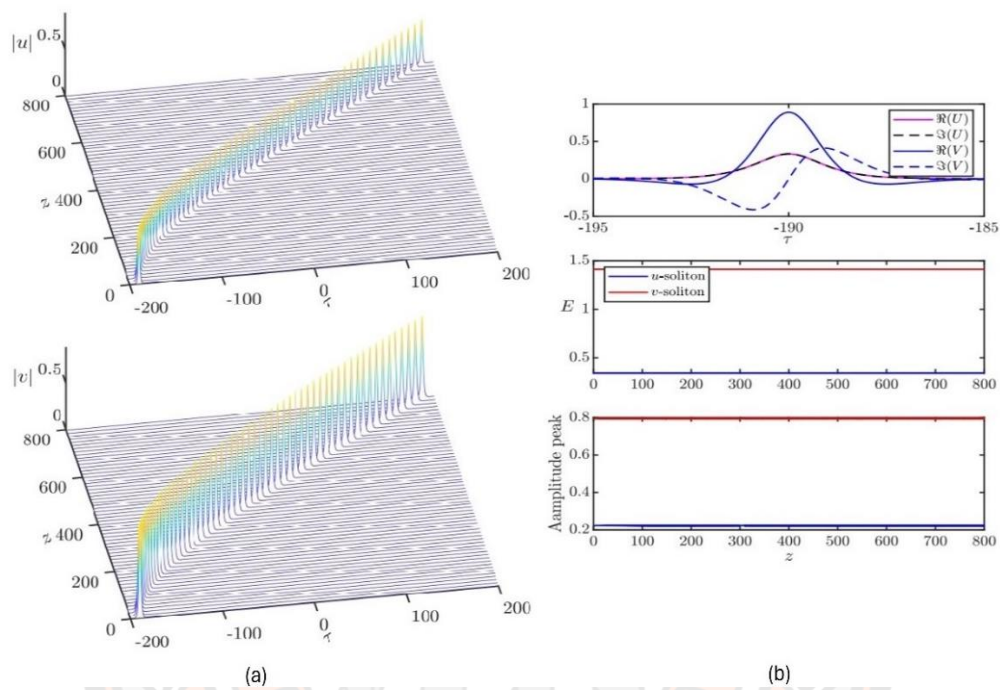
Figure 21 (a) The stable *u*-soliton (Left top) and *v*-soliton (Left bottom). (b) (Right top) The profiles of the initial solutions at z = 0, (middle) the energy of solitons vs. z, (bottom) the amplitude peak vs. z for $c = 0.9$ and $\alpha = 2.0$.
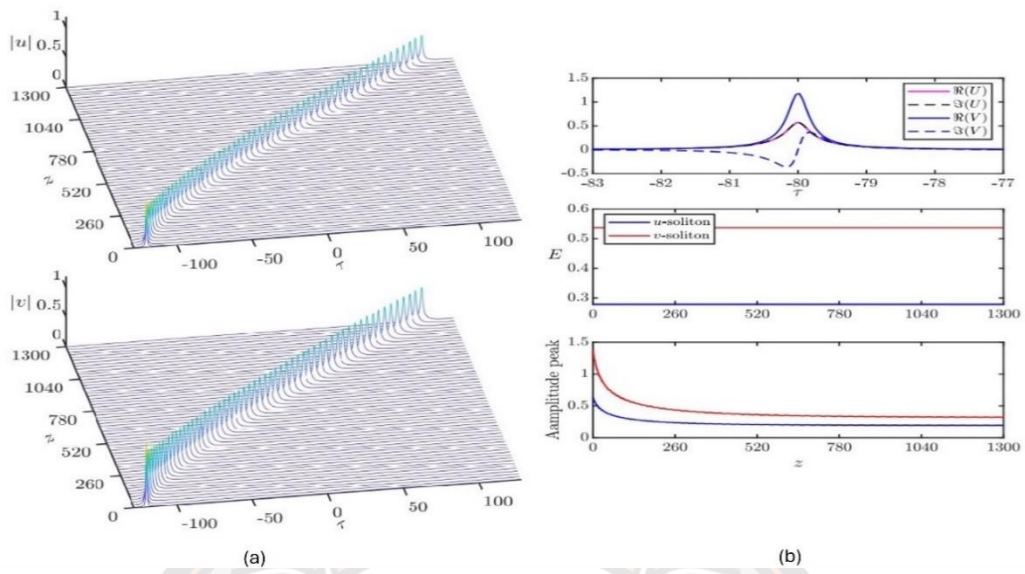
Figure 22 (a)The stable *u*-soliton (Left top) and *v*-soliton (Left bottom). (b) (Right top) The profiles of the initial solutions at z = 0, (middle) the energy of solitons vs. z, (bottom) the amplitude peak vs. z for $c = 0.4$ and $\alpha = 1.1$.
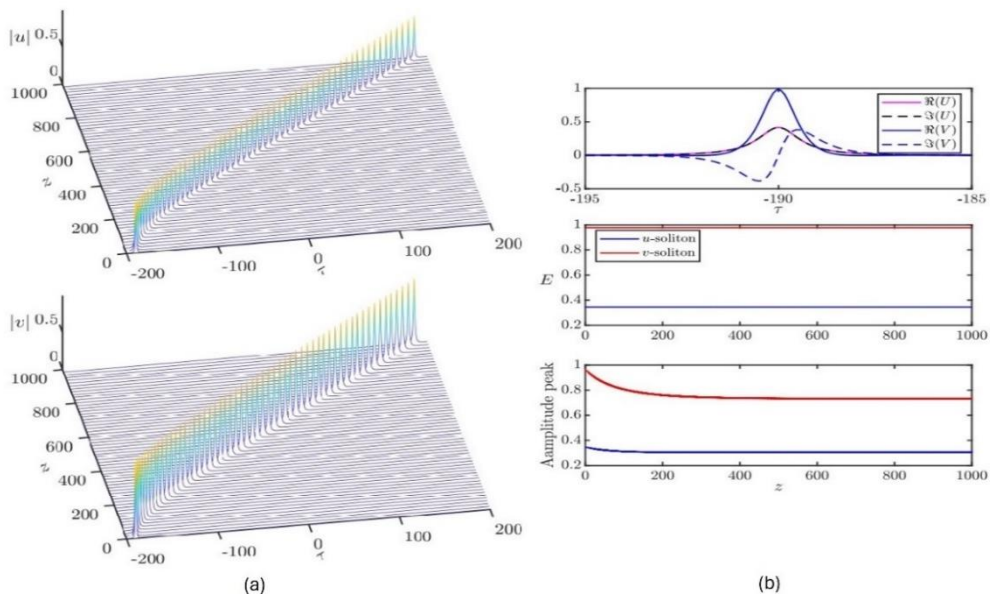
Figure 23 (a) The stable *u*-soliton (Left top) and *v*-soliton (Left bottom). (b) (Right top) The profiles of the initial solutions at z = 0, (middle) the energy of solitons vs. z, (bottom) the amplitude peak vs. z for $c = 0.7$ and $\alpha = 1.5$.

4.5 Summary of the collisions of two bound states of solitons.

The energies of the solitons are different for different values of α and are influenced by values of the GV mismatch factor, i.e., c. Figure 23 below displays the impacts of c on energy E for different values of α.

For higher LI, α = 2, the energy is highest compared to all other values and the velocity increases from 0 to 1, the energy of v-soliton increases exponentially whereas the energy of u-soliton decreases exponentially in the same manner.

For α = 1.5, the energies of both u- and v-solitons increase and decrease respectively in a similar manner as α = 2, but the changes are very slow and stop at c = 0.8.

For α = 1.1, the energies of u-soliton are almost linear with negligible increase with c whereas v-soliton decreases gradually. Both the energies stop at c = 0.5.

It can be concluded that, since the velocity of the u-soliton is fixed at 0, the energy increases as the velocity, c increases from 0 to. However, v-soliton is a different case, since it moves towards u-soliton while travelling, its energies decrease with c but does not reach 0. So, these changes in the energies are very small and negligible and as a result, the energy is conserved.
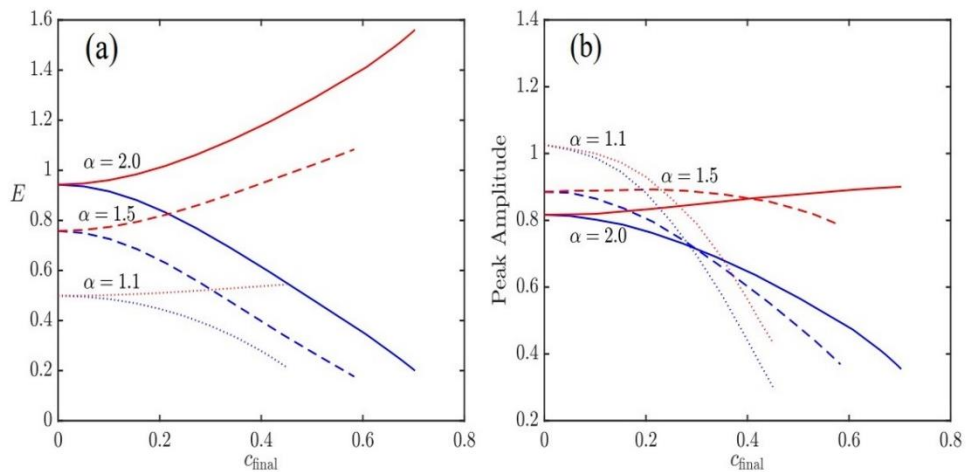
Figure 24 The energies (a) and amplitudes (b) of the established u- and v-components (blue and red curves, respectively) of the compound solitons vs. their established rapidity, c_{final}, for the same value of LI, used in the above figures.
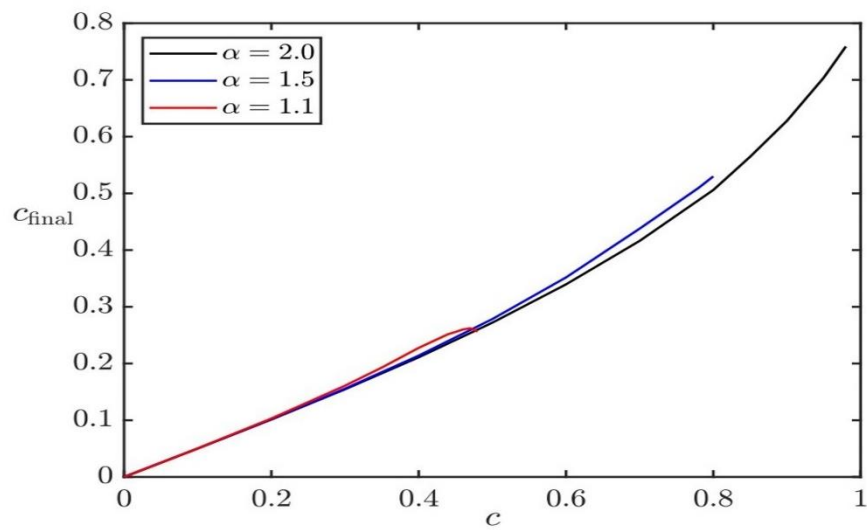
Figure 25 The final rapidity of the established two-component soliton, c_final, vs. the GV mismatch parameter c for three values of LI, $\alpha = 2$ (the ordinary non-fractional GVD), $\alpha = 1.5$ (moderate fractionality), and $\alpha = 1.1$ (strong fractionality).

CHAPTER V

CONCLUSION AND FUTURE WORKS

5.1 Conclusion

In this final chapter, we draw conclusions based on the findings presented in Chapter 4 regarding the collisions between two fractional solitons. Additionally, we discuss potential avenues for future research aimed at expanding our understanding of soliton dynamics and their applications.

The investigation of fractional solitons' collisions has yielded important insights into the nonlinear interactions of these structures. We have evaluated the stability of collision-induced patterns, recognized different collision results, and tracked the evolution of soliton profiles using graphical representations and analysis. The results of this study enhance the overall comprehension of soliton dynamics and their conduct in the context of collision situations.

By mentioning WDM environment, it's worth noting that for this study, in the assumed laser cavities, the existence and copropagating of two fractional solitons with fractional dispersion with SPM and XPM as nonlinear terms can be understood as passive system. The main goal is to investigate the effects of fractional dispersion, SPM and XPM on fractional solitons during co-propagating and the outcomes of those solitons colliding with each other and how it's different than standard system with ordinary dispersion of ordinary solitons. The outcomes of the fractional solitons' collisions are compared with ordinary solitons using same parameter variations of α and velocity mismatch. The simulated results show that when $\alpha = 2$ (now becomes standard system) has only two outcomes namely splitting (inelastic) and elastic as velocity mismatch $c > 2.6$. As α decreases or as fractionality increases, variations of outcomes are observed such as repulsion, merger into single exhibiting breather-like amplitude profile, splitting and finally into quasi-elastic as c increases. The numerically found solutions using MSOM when compared (plotted for $\alpha = 2$ and $k = 1$) with the available analytical solutions are observed to be exactly same further confirming the accuracy of the adopted numerical method. The bound state of two fractional solitons

by incorporating the effects of XPM when co-propagating with initial velocity is observed to accelerate initially followed by deceleration after certain distance which becomes constant and termed as final velocity.

In the fibre cavity with the effective FGVD (fractional group-velocity dispersion), which is currently accessible for experimentation, we have also taken into consideration the co-propagation of optical pulses that are carried by the light of varying wavelengths. The system is represented by the XPM-coupled system of FNLSEs, where the FGVD is described by the Riesz fractional derivatives. The Lévy index, denoted as α, has values between 1 and 2 (inclusive), with $\alpha = 2$ corresponding to the ordinary non-fractional GVD. The system comprises the SPM nonlinear terms and the group-velocity (GV) mismatch c to study the fractional solitons collision and addition of XPM nonlinear terms to study the bound state of two fractional solitons.

The numerical findings presented in this paper illustrate the numerically found fractional soliton solutions and their co-propagating dynamics.

5.2 Future works

Several scientific and technical fields will be impacted by the study's findings. Since solitons are resistant to dispersion effects, they are used for signal transmission in modern optical communication systems; hence, an understanding of soliton collisions is essential. This work also has applications in the domains of fluid dynamics, plasma physics, and nonlinear optics, where soliton-like phenomena are observed. Furthermore, the investigation of soliton collisions enhances our comprehension of complex dynamical systems by contributing to foundational research on nonlinear wave interactions.

The next research step would be to incorporate an additional significant nonlinear factor, such as Four Wave Mixing (FWM), to examine its influence on the collision of the fractional solitons. Furthermore, the omission of characteristics such as loss and amplification (gain) in the fibre cavity in this research opens new avenues for further exploration of the subject.

Although the findings given in this thesis offer interesting insights, it is important to acknowledge several limitations that should be considered for future research. A weakness of the study is its narrow focus on collisions involving only two

fractional solitons, which may not encompass the entirety of collision scenarios observed in complicated nonlinear systems. Further research could investigate collisions that involve several soliton-like structures or interactions in nonlinear media with different characteristics. Furthermore, this thesis primarily emphasizes numerical simulations in its study. Conducting experiments to confirm the collision dynamics found in simulations would increase the dependability and practicality of the results. Furthermore, studying the impact of external disturbances, such as noise or disruptions, on soliton collisions could offer an additional understanding of the resilience of soliton-like structures in real-life situations.

Overall, the investigation into the collisions of fractional solitons has yielded a significant understanding of the dynamics of soliton interactions. The outcomes detailed in this thesis make a valuable contribution to the progression of knowledge regarding nonlinear wave phenomena and carry significant implications for a wide range of scientific and technological implementations. Moving forward, more research efforts aimed at examining various collision scenarios, experimental validation, and investigating the impacts of external perturbations will improve our understanding of soliton dynamics and possible applications.

REFERENCES

Agrawal, G. P. (2000). Nonlinear fiber optics. In *Nonlinear Science at the Dawn of the 21st Century* (pp. 195-211). Springer.

Agrawal, G. P. (2019). Chapter 7 - Cross-phase modulation. In G. P. Agrawal (Ed.), *Nonlinear Fiber Optics (Sixth Edition)* (pp. 245-295). Academic Press. https://doi.org/https://doi.org/10.1016/B978-0-12-817042-7.00014-2

Al-Raeei, M., & El-Daher, M. S. (2020). An algorithm for fractional Schrödinger equation in case of Morse potential. *AIP Advances*, *10*(3). https://doi.org/10.1063/1.5113593

Alhorani, M., & Khalil, R. (2018). Total fractional differentials with applications to exact fractional differential equations. *International Journal of Computer Mathematics*, *95*, 1444 - 1452.

Ali, K. K., & Maneea, M. (2023). Optical soliton solutions for space fractional Schrödinger equation using similarity method. *Results in Physics*, *46*, 106284. https://doi.org/https://doi.org/10.1016/j.rinp.2023.106284

Alquran, M., Jaradat, I., & Baleanu, D. (2019). Shapes and dynamics of dual-mode Hirota–Satsuma coupled KdV equations: Exact traveling wave solutions and analysis. *Chinese Journal of Physics*, *58*, 49-56. https://doi.org/https://doi.org/10.1016/j.cjph.2019.01.005

Alshehry, A. S., Shah, R., Shah, N. A., & Dassios, I. K. (2022). A Reliable Technique for Solving Fractional Partial Differential Equation. *Axioms*, *11*, 574.

Bhrawy, A. H., Alshaery, A. A., Hilal, E. M., Jovanoski, Z., & Biswas, A. (2014). Bright and dark solitons in a cascaded system. *Optik*, *125*(20), 6162-6165. https://doi.org/https://doi.org/10.1016/j.ijleo.2014.06.118

Biswas, A., Mirzazadeh, M., Eslami, M., Zhou, Q., Bhrawy, A., & Belic, M. (2016). Optical solitons in nano-fibers with spatio-temporal dispersion by trial solution method. *Optik*, *127*(18), 7250-7257. https://doi.org/https://doi.org/10.1016/j.ijleo.2016.05.052

Bulut, H., Sulaiman, T. A., & Baskonus, H. M. (2018). On the solitary wave solutions to the longitudinal wave equation in MEE circular rod. *Optical and Quantum Electronics*, *50*, 1-10.

Cai, M., & Li, C. (2019). On Riesz Derivative. *Fractional Calculus and Applied Analysis*, *22*(2), 287-301. https://doi.org/10.1515/fca-2019-0019

Cao, Q.-H., & Dai, C.-Q. (2021). Symmetric and Anti-Symmetric Solitons of the Fractional Second- and Third-Order Nonlinear Schrödinger Equation. *Chinese Physics Letters*, *38*(9), 090501. https://doi.org/10.1088/0256-307X/38/9/090501

Chen, C., & Jiang, Y. (2018). Simplest equation method for some time-fractional partial differential equations with conformable derivative. *Comput. Math. Appl.*, *75*, 2978-2988.

Chen, M., Guo, Q., Lu, D., & Hu, W. (2019). Variational approach for breathers in a nonlinear fractional Schrödinger equation. *Communications in Nonlinear Science and Numerical Simulation*, *71*, 73-81. https://doi.org/https://doi.org/10.1016/j.cnsns.2018.11.013

Cheung, T. Y. (1979). Newton's method for nonlinear ordinary and partial differential

equations. *Journal of Mathematical Analysis and Applications*, *70*, 474-485.

Diethelm, K., & Ford, N. J. (2002). Analysis of Fractional Differential Equations. *Journal of Mathematical Analysis and Applications*, *265*(2), 229-248. https://doi.org/https://doi.org/10.1006/jmaa.2000.7194

Dong, J., & Xu, M. (2007). Some solutions to the space fractional Schrödinger equation using momentum representation method. *Journal of Mathematical Physics*, *48*(7). https://doi.org/10.1063/1.2749172

Esen, A., Sulaiman, T. A., Bulut, H., & Baskonus, H. M. (2018). Optical solitons to the space-time fractional (1+1)-dimensional coupled nonlinear Schrödinger equation. *Optik*, *167*, 150-156. https://doi.org/https://doi.org/10.1016/j.ijleo.2018.04.015

Farag, N. G. A., Eltanboly, A. H., El-Azab, M. S., & Obayya, S. S. A. (2021). On the Analytical and Numerical Solutions of the One-Dimensional Nonlinear Schrodinger Equation. *Mathematical Problems in Engineering*, *2021*, 3094011. https://doi.org/10.1155/2021/3094011

Felmer, P., Quaas, A., & Tan, J. (2012). Positive solutions of the nonlinear Schrödinger equation with the fractional Laplacian [Article]. *Royal Society of Edinburgh - Proceedings A*, *142*(6), 1237-1262. https://doi.org/10.1017/S0308210511000746

Feng, Q., & Meng, F. (2017). Traveling wave solutions for fractional partial differential equations arising in mathematical physics by an improved fractional Jacobi elliptic equation method. *Mathematical Methods in the Applied Sciences*, *40*, 3676 - 3686.

Feng, Y., & Ma, D. (2023). Numerical Solution for a Fractional Differential Equation Arising In Optics. *Journal of Physics: Conference Series*, *2597*(1), 012011. https://doi.org/10.1088/1742-6596/2597/1/012011

Feynman, R. P., & Hibbs, A. R. (1965). Quantum Mechanics and Path Integrals.

Fujioka, J., Espinosa, A., & Rodríguez, R. F. (2010). Fractional optical solitons. *Physics Letters A*, *374*(9), 1126-1134. https://doi.org/https://doi.org/10.1016/j.physleta.2009.12.051

Ghalandari, M., & Solaimani, M. (2019). Wave transport in fractional Schrodinger equations. *Optical and Quantum Electronics*, *51*.

Ghosh, S., & Nandy, S. (1999). Inverse scattering method and vector higher order non-linear Schrödinger equation. *Nuclear Physics*, *561*, 451-466.

Guo, X., & Jiang, X. (2006). Some physical applications of fractional Schrödinger equation. *Journal of Mathematical Physics*, *47*, 082104-082104. https://doi.org/10.1063/1.2235026

Haus, H. A. (1975). Theory of Mode Locking with a Slow Saturable Absorber [Article]. *IEEE Journal of Quantum Electronics*, *11*(9), 736-746. https://doi.org/10.1109/JQE.1975.1068922

Huang, C., & Dong, L. (2016). Gap solitons in the nonlinear fractional Schrödinger equation with an optical lattice. *Optics Letters*, *41 24*, 5636-5639.

Huang, X., Deng, Z., & Fu, X. (2017). Dynamics of finite energy Airy beams modeled by the fractional Schrödinger equation with a linear potential. *Journal of The Optical Society of America B-optical Physics*, *34*, 976-982.

Kasai, Y., Aizawa, T., & Tanaka, D. (2018). *High-power fiber-coupled pump lasers for fiber lasers* (Vol. 10514). SPIE. https://doi.org/10.1117/12.2288139

Kasai, Y., Yamagata, Y., Kaifuchi, Y., Sakamoto, A., & Tanaka, D. (2017). High-brightness and high-efficiency fiber-coupled module for fiber laser pump with advanced laser diode. High-Power Diode Laser Technology XV,

Keren-Zur, S., Michaeli, L., Suchowski, H., & Ellenbogen, T. (2018). Shaping light with nonlinear metasurfaces. *Advances in Optics and Photonics*, *10*(1), 309-353. https://doi.org/10.1364/AOP.10.000309

Khanikaev, A. B., Hossein Mousavi, S., Tse, W.-K., Kargarian, M., MacDonald, A. H., & Shvets, G. (2013). Photonic topological insulators. *Nature Materials*, *12*(3), 233-239. https://doi.org/10.1038/nmat3520

Kilbas, A. A., Srivastava, H. M., & Trujillo, J. J. (2006). Theory and Applications of Fractional Differential Equations.

Kurt, A. S., Tasbozan, O., & Durur, H. (2019). The Exact Solutions of Conformable Fractional Partial Differential Equations Using New Sub Equation Method.

Lakshmikantham, V., & Vatsala, A. S. (2008). Basic theory of fractional differential equations. *Nonlinear Analysis: Theory, Methods & Applications*, *69*(8), 2677-2682. https://doi.org/https://doi.org/10.1016/j.na.2007.08.042

Laskin, N. (2000). Fractional quantum mechanics and Lévy path integrals. *Physics Letters A*, *268*(4), 298-305. https://doi.org/https://doi.org/10.1016/S0375-9601(00)00201-2

Laskin, N. (2002). Fractional Schrödinger equation. *Physical review. E, Statistical, nonlinear, and soft matter physics*, *66 5 Pt 2*, 056108.

Laskin, N. (2008). Fractional quantum mechanics. *Physical review. E, Statistical physics, plasmas, fluids, and related interdisciplinary topics*, *62 3 Pt A*, 3135-3145.

Liu, S., Zhang, Y., Malomed, B. A., & Karimi, E. (2023). Experimental realisations of the fractional Schrödinger equation in the temporal domain. *Nature Communications*, *14*(1), 222.

Longhi, S. (2015). Fractional Schrödinger equation in optics. *Optics Letters*, *40*(6), 1117-1120. https://doi.org/10.1364/OL.40.001117

Malomed, B. A. (2021). Optical Solitons and Vortices in Fractional Media: A Mini-Review of Recent Results. *Photonics*, *8*, 353.

Mehboob, A. B., Usman, M., & Hussain, A. (2019). Generation and transmission of fractional-order optical bright solitons in single mode fiber. *Microwave and Optical Technology Letters*, *61*(12), 2886-2900. https://doi.org/https://doi.org/10.1002/mop.31953

Miller, K. S., & Ross, B. (1993). An Introduction to the Fractional Calculus and Fractional Differential Equations.

Monmayrant, A., Weber, S. J., & Chatel, B. e. (2010). PhD TUTORIAL: A newcomer's guide to ultrashort pulse shaping and characterization. *Journal of Physics B*.

Naber, M. G. (2004). Time fractional Schrödinger equation. *Journal of Mathematical Physics*, *45*, 3339-3352.

Nishimoto, K. (1984). *Fractional calculus: integrations and differentiations of arbitrary order* (Vol. 5). Descartes Press.

Odabasi, M., & Mısırlı, E. (2018). On the solutions of the nonlinear fractional differential equations via the modified trial equation method. *Mathematical*

Methods in the Applied Sciences, *41*, 904 - 911.

Oldham, K. B., & Spanier, J. (1974). The Fractional Calculus: Theory and Applications of Differentiation and Integration to Arbitrary Order.

Ortigueira, M. (2011). *Fractional Calculus for Scientist and Engineers* (Vol. 84). https://doi.org/10.1007/978-94-007-0747-4

Petviashvili, V. I. (1976). Equation of an extraordinary soliton. *Soviet journal of plasma physics*, *2*, 257.

Podlubny, I. (1999). Fractional differential equations : an introduction to fractional derivatives, fractional differential equations, to methods of their solution and some of their applications.

Pu, Y.-f., Siarry, P., Zhou, J., & Zhang, N. (2014). A fractional partial differential equation based multiscale denoising model for texture image. *Mathematical Methods in the Applied Sciences*, *37*.

Qiu, Y., Malomed, B. A., Mihalache, D., Zhu, X., Peng, X., & He, Y. (2020). Stabilization of single- and multi-peak solitons in the fractional nonlinear Schrödinger equation with a trapping potential. *Chaos Solitons & Fractals*, *140*, 110222.

Rezazadeh, H. (2018). New solitons solutions of the complex Ginzburg-Landau equation with Kerr law nonlinearity. *Optik*, *167*, 218-227. https://doi.org/https://doi.org/10.1016/j.ijleo.2018.04.026

Siegman, A. E. (1986). *Lasers*. University science books.

Stickler, B. (2013). Potential condensed-matter realization of space-fractional quantum mechanics: The one-dimensional Levy crystal. *Physical review. E, Statistical, nonlinear, and soft matter physics*, *88*, 012120. https://doi.org/10.1103/PhysRevE.88.012120

Turitsyn, S. K. (2009). Theory of energy evolution in laser resonators with saturated gain and non-saturated loss [Article]. *Optics Express*, *17*(14), 11898-11904. https://doi.org/10.1364/OE.17.011898

Turitsyn, S. K., Bale, B. G., & Fedoruk, M. P. (2012). Dispersion-managed solitons in fibre systems and lasers. *Physics Reports*, *521*(4), 135-203. https://doi.org/https://doi.org/10.1016/j.physrep.2012.09.004

Vázquez, L., Trujillo, J. J., & Pilar Velasco, M. (2011). Fractional heat equation and the second law of thermodynamics. *Fractional Calculus and Applied Analysis*, *14*(3), 334-342. https://doi.org/10.2478/s13540-011-0021-9

Wang, H., & Zheng, X. (2019). Analysis and numerical solution of a nonlinear variable-order fractional differential equation. *Advances in Computational Mathematics*, *45*, 2647 - 2675.

Wang, S., & Jiang, X. (2007). Generalized fractional Schrödinger equation with space-time fractional derivatives. *Journal of Mathematical Physics*, *48*, 043502-043502. https://doi.org/10.1063/1.2716203

Weiner, A. M. (2011). Ultrafast optical pulse shaping: A tutorial review. *Optics Communications*, *284*(15), 3669-3692. https://doi.org/https://doi.org/10.1016/j.optcom.2011.03.084

Wu, G.-Z., Yu, L.-J., & Wang, Y.-Y. (2020). Fractional optical solitons of the space-time fractional nonlinear Schrödinger equation. *Optik*, *207*, 164405. https://doi.org/https://doi.org/10.1016/j.ijleo.2020.164405

Yang, J. (2002). Internal oscillations and instability characteristics of (2+1)-dimensional solitons in a saturable nonlinear medium. *Physical review. E, Statistical, nonlinear, and soft matter physics*, *66 2 Pt 2*, 026601.

Yang, J., & Lakoba, T. I. (2007). Universally-Convergent Squared-Operator Iteration Methods for Solitary Waves in General Nonlinear Wave Equations. *Studies in Applied Mathematics*, *118*.

Yarutkina, I. A., Shtyrina, O. V., Skidin, A., & Fedoruk, M. P. (2015). Theoretical study of energy evolution in ring cavity fiber lasers. *Optics Communications*, *342*, 26-29. https://doi.org/https://doi.org/10.1016/j.optcom.2014.12.050

Zhai, H. (2015). Degenerate quantum gases with spin–orbit coupling: a review. *Reports on Progress in Physics*, *78*(2), 026001. https://doi.org/10.1088/0034-4885/78/2/026001

Zhang, L., Li, C., Zhong, H., Xu, C., Lei, D., Li, Y., & Fan, D. (2016). Propagation dynamics of super-Gaussian beams in fractional Schrödinger equation: From linear to nonlinear regimes [Article]. *Optics Express*, *24*(13), 14406-14418. https://doi.org/10.1364/OE.24.014406

Zhang, Y., Liu, X., Belić, M. R., Zhong, W.-P., Zhang, Y., & Xiao, M. (2015). Propagation Dynamics of a Light Beam in a Fractional Schrödinger Equation. *Physical review letters*, *115 18*, 180403.

APPENDIX

CASE I: Finding the soliton solution using MSOM.

```matlab
clear all; close all;

T=60; nfft=2^12;                          % grid parameters
ds=T/nfft;
s=[-T/2:ds:T/2-ds];
freq=(2*pi/T)*[0:nfft/2];
w=[freq(1:nfft/2),-freq(nfft/2+1:-1:2)];

max_iteration=1e5; error_tolerance=1e-10;
%===========================
alph = 2;
w_alpha=(w.^2).^(alph/2);
tau=1;
%===========================
c=3.8; DT=0.6;

k=-1;

A=1;
U=A*exp(-1*(s-0).^2);
V=A*exp(-1*(s-8).^2);

for nn=1:max_iteration                              % MSOM iterations start
    Uold=U;
    Vold=V;

    L0U=1/2*ifft((-w_alpha).*fft(U))+k.*U + U.*(U.^2);
    L0V=1/2*ifft((-w_alpha).*fft(V))+k.*V + V.*(V.^2);

    MinvL0U=ifft(fft(L0U)./(1/2*(w_alpha)+c));
    MinvL0V=ifft(fft(L0V)./(1/2*(w_alpha)+c));

L1HermitMinvL0U=1/2*ifft((w_alpha).*fft(MinvL0U))+k.*MinvL0U+(3*U.^2).*Minv
L0U;
L1HermitMinvL0V=1/2*ifft((w_alpha).*fft(MinvL0V))+k.*MinvL0V+(3*V.^2).*Minv
L0V;

    MinvL1HermitMinvL0U=ifft(fft(L1HermitMinvL0U)./(1/2*(w_alpha)+c));
    MinvL1HermitMinvL0V=ifft(fft(L1HermitMinvL0V)./(1/2*(w_alpha)+c));
    if nn == 1
        U=U-MinvL1HermitMinvL0U*DT;
        V=V-MinvL1HermitMinvL0V*DT;
    else
        L1G1=1/2*ifft(-w_alpha.*fft(G1))+k.*G1+(3*U.^2).*G1;
        L1G2=1/2*ifft(-w_alpha.*fft(G2))+k.*G2+(3*V.^2).*G2;

        MinvL1G1=ifft(fft(L1G1)./(1/2*(w_alpha)+c));
        MinvL1G2=ifft(fft(L1G2)./(1/2*(w_alpha)+c));
```

```
        MG1=ifft(fft(G1).*(1/2*(w_alpha)+c));
        MG2=ifft(fft(G2).*(1/2*(w_alpha)+c));

        alpha1=1/sum(conj(MG1).*G1+conj(MG2).*G2)-
1/(DT*sum(conj(L1G1).*MinvL1G1+conj(L1G2).*MinvL1G2));


innerproduct=sum(real(G1).*real(L1HermitMinvL0U)+imag(G1).*imag(L1HermitMin
vL0U)+real(G2).*real(L1HermitMinvL0V)+imag(G2).*imag(L1HermitMinvL0V));


        U=U-(MinvL1HermitMinvL0U-alpha1*innerproduct*G1)*DT;
        V=V-(MinvL1HermitMinvL0V-alpha1*innerproduct*G2)*DT;
    end
    G1=U-Uold;
    G2=V-Vold;
    Uerror(nn)=sqrt(sum(abs(U-Uold).^2))*ds; Uerror(nn)
    if Uerror(nn) < error_tolerance
        break
    end
end
 Power = sum(abs(U).^2+abs(V).^2)*ds
 Power = sum(abs(U).^2)*ds
 Peak=max(abs(U).^2)
 u_analyt = sqrt(2)*sech(sqrt(2)*s);
figure(1), plot(s,abs(U),'r',s,abs(V),'b-') %,s,abs(u_analyt).^2,'--k'
 xlabel('\tau'), ylabel('')%legend('U','Exact solitons')

figure(6), semilogy(1:length(Uerror), Uerror, 'linewidth', 2)
%xlabel('number of CG iterations', 'fontsize', 16); ylabel('error',
'fontsize', 16)
```

CASE II: Numerical solution for bound state solitons

```
clear all; close all;

T=256; nfft=2^12;                          % grid parameters
ds=T/nfft;
s=[-T/2:ds:T/2-ds];
freq=(2*pi/T)*[0:nfft/2];
w=[freq(1:nfft/2),-freq(nfft/2+1:-1:2)];

max_iteration=1e5; error_tolerance=2e-9;
%=========================
alph = 1.1;
w_alpha=(w.^2).^(alph/2);
tau=1;
%=========================
c=5.8; DT=0.6;
k=-1;
```

```matlab
pos=110;
vel=0.45;

Au=0.38;
Av=Au;
Ur=Au*exp(-1*(s+pos).^2);
Ui=Au*exp(-1*(s+pos).^2)
Vr=Av*exp(-1*(s+pos).^2);
Vi=Av*exp(-1*(s+pos).^2).*sin(s+pos);

for nn=1:max_iteration                          % MSOM iterations start
    Urold=Ur;
    Uiold=Ui;
    Vrold=Vr;
    Viold=Vi;


L0Ur=1/2*ifft((w_alpha).*fft(Ur))+k.*Ur+(Ur.^2+Ui.^2+2*(Vr.^2+Vi.^2)).*Ur;
L0Ui=1/2*ifft((w_alpha).*fft(Ui))+k.*Ui+(Ur.^2+Ui.^2+2*(Vr.^2+Vi.^2)).*Ui;

L0Vr=1/2*ifft((w_alpha).*fft(Vr))+vel*ifft(1i*w.*fft(Vi))+k.*Vr+(2*(Ur.^2+U
i.^2)+Vr.^2+Vi.^2).*Vr;

L0Vi=1/2*ifft((w_alpha).*fft(Vi))vel*ifft(1i*w.*fft(Vr))+k.*Vi+(2*(Ur.^2+Ui
.^2)+Vr.^2+Vi.^2).*Vi;

    MinvL0Ur=ifft(fft(L0Ur)./(1/2*(w_alpha)+c));
    MinvL0Ui=ifft(fft(L0Ui)./(1/2*(w_alpha)+c));
    MinvL0Vr=ifft(fft(L0Vr)./(1/2*(w_alpha)+c));
    MinvL0Vi=ifft(fft(L0Vi)./(1/2*(w_alpha)+c));


L1HermitMinvL0Ur=1/2*ifft((w_alpha).*fft(MinvL0Ur))+(k+3*Ur.^2+Ui.^2+2*(Vr.
^2+Vi.^2)).*MinvL0Ur+2*Ur.*Ui.*MinvL0Ui+4*Ur.*Vr.*MinvL0Vr+4*Ur.*Vi.*MinvL0
Vi;

L1HermitMinvL0Ui=1/2*ifft((w_alpha).*fft(MinvL0Ui))+(k+3*Ui.^2+Ur.^2+2*(Vr.
^2+Vi.^2)).*MinvL0Ui+2*Ur.*Ui.*MinvL0Ur+4*Ui.*Vr.*MinvL0Vr +
4*Ui.*Vi.*MinvL0Vi;

L1HermitMinvL0Vr=1/2*ifft((w_alpha).*fft(MinvL0Vr))vel*ifft(1i*w.*fft(MinvL
0Vi))+(k+3*Vr.^2+Vi.^2+2*(Ur.^2+Ui.^2)).*MinvL0Vr+4*Vr.*Ur.*MinvL0Ur+4*Vr.*
Ui.*MinvL0Ui+2*Vr.*Vi.*MinvL0Vi;

L1HermitMinvL0Vi=1/2*ifft((w_alpha).*fft(MinvL0Vi))+vel*ifft(1i*w.*fft(Minv
L0Vr))+(k+3*Vi.^2+Vr.^2+2*(Ur.^2+Ui.^2)).*MinvL0Vi+4*Vi.*Ur.*MinvL0Ur+4*Vi.
*Ui.*MinvL0Ui+2*Vi.*Vr.*MinvL0Vr;

    MinvL1HermitMinvL0Ur=ifft(fft(L1HermitMinvL0Ur)./(1/2*(w_alpha)+c));
    MinvL1HermitMinvL0Ui=ifft(fft(L1HermitMinvL0Ui)./(1/2*(w_alpha)+c));
    MinvL1HermitMinvL0Vr=ifft(fft(L1HermitMinvL0Vr)./(1/2*(w_alpha)+c));
    MinvL1HermitMinvL0Vi=ifft(fft(L1HermitMinvL0Vi)./(1/2*(w_alpha)+c));
    if nn == 1
        Ur=Ur-MinvL1HermitMinvL0Ur*DT;
        Ui=Ui-MinvL1HermitMinvL0Ui*DT;
        Vr=Vr-MinvL1HermitMinvL0Vr*DT;
```

```
        Vi=Vi-MinvL1HermitMinvL0Vi*DT;
    else

L1G1=1/2*ifft(w_alpha.*fft(G1))+(k+3*Ur.^2+Ui.^2+2*(Vr.^2+Vi.^2)).*G1+2*Ur.
*Ui.*G2 + 4*Ur.*Vr.*G3 + 4*Ur.*Vi.*G4; %G1=Ur

L1G2=1/2*ifft(w_alpha.*fft(G2))+(k+3*Ui.^2+Ur.^2+2*(Vr.^2+Vi.^2)).*G2+2*Ur.
*Ui.*G1 + 4*Ui.*Vr.*G3 + 4*Ui.*Vi.*G4; %G2=Ui

L1G3=1/2*ifft(w_alpha.*fft(G3))vel*ifft(1i*w.*fft(G4))+(k+3*Vr.^2+Vi.^2+2*(
Ur.^2+Ui.^2)).*G3+4*Vr.*Ur.*G1+4*Vr.*Ui.*G2+2*Vr.*Vi.*G4; %G3=Vr

L1G4=1/2*ifft(w_alpha.*fft(G4))+vel*ifft(1i*w.*fft(G3))+(k+3*Vi.^2+Vr.^2+2*
(Ur.^2+Ui.^2)).*G4+4*Vi.*Ur.*G1+4*Vi.*Ui.*G2+2*Vi.*Vr.*G3; %G4=Vi

        MinvL1G1=ifft(fft(L1G1)./(1/2*(w_alpha)+c));
        MinvL1G2=ifft(fft(L1G2)./(1/2*(w_alpha)+c));
        MinvL1G3=ifft(fft(L1G3)./(1/2*(w_alpha)+c));
        MinvL1G4=ifft(fft(L1G4)./(1/2*(w_alpha)+c));

        MG1=ifft(fft(G1).*(1/2*(w_alpha)+c));
        MG2=ifft(fft(G2).*(1/2*(w_alpha)+c));
        MG3=ifft(fft(G3).*(1/2*(w_alpha)+c));
        MG4=ifft(fft(G4).*(1/2*(w_alpha)+c));


alpha1=1/sum(conj(MG1).*G1+conj(MG2).*G2+conj(MG3).*G3+conj(MG4).*G4)1/(DT*
sum(conj(L1G1).*MinvL1G1+conj(L1G2).*MinvL1G2+conj(L1G3).*MinvL1G3+conj(L1G
4).*MinvL1G4));


innerproduct=sum(real(G1).*real(L1HermitMinvL0Ur)+imag(G1).*imag(L1HermitMi
nvL0Ur)+real(G2).*real(L1HermitMinvL0Ui)+imag(G2).*imag(L1HermitMinvL0Ui)+r
eal(G3).*real(L1HermitMinvL0Vr)+imag(G3).*imag(L1HermitMinvL0Vr)+real(G4).*
real(L1HermitMinvL0Vi)+imag(G4).*imag(L1HermitMinvL0Vi));

        Ur=Ur-(MinvL1HermitMinvL0Ur-alpha1*innerproduct*G1)*DT;
        Ui=Ui-(MinvL1HermitMinvL0Ui-alpha1*innerproduct*G2)*DT;
        Vr=Vr-(MinvL1HermitMinvL0Vr-alpha1*innerproduct*G3)*DT;
        Vi=Vi-(MinvL1HermitMinvL0Vi-alpha1*innerproduct*G4)*DT;
    end
    G1=Ur-Urold;
    G2=Ui-Uiold;
    G3=Vr-Vrold;
    G4=Vi-Viold;

    Uerror(nn)=sqrt(sum(abs(Ur-Urold).^2+abs(Ui-Uiold).^2+abs(Vr-
Vrold).^2+abs(Vi-Viold).^2))*ds; Uerror(nn)
    if Uerror(nn) < error_tolerance
        break
    end
end

 U=Ur+i*Ui;
 V=Vr+i*Vi;
```

```
EU = sum(abs(U).^2)*ds
EV = sum(abs(V).^2)*ds
E = sum(abs(U).^2+abs(V).^2)*ds
uv_analytic = sqrt(2/3)*sech(sqrt(2)*s);
E_analytic = sum(abs(uv_analytic).^2)*ds
Peaku=max(abs(U))
Peakv=max(abs(V))
figure(1),
pos1 = [0.22 0.55 0.7 0.3];
subplot('position',pos1)
plot(s,real(U),'-m',s,imag(U),'--k',s,real(V),'-b',s,imag(V),'--b'),
xlim([-115 -105])
xlabel('$\tau$'),
legend('$\Re{(U)}$','$\Im{(U)}$','$\Re{(V)}$','$\Im{(V)}$')

figure(6), semilogy(1:length(Uerror), Uerror, 'linewidth', 2)
```

CASE III: Direct simulation for the evolution of soliton collision (Split Step Fourier   Transform)

```
clear all; close all;

load 'H:\MATLAB Research\Fractional Fiber Laser\Collision
Solitons\FracSolUV.mat'
%T=1024; nfft=2^13;                              % grid parameters

L = 60;
dz = 0.001;
step=100;
z= [0:dz:L];
ds=T/nfft;
s=[-T/2:ds:T/2-ds];
freq=(2*pi/T)*[0:nfft/2];
w=[freq(1:nfft/2),-freq(nfft/2+1:-1:2)];
%========== Physical Units =====================
t=1; %ps
xi=10; %m
gamma=50; %W
%=================== damping edge ===============================
sdamp=[0:ds:2*ds];
negdamp=exp(-(sdamp(length(sdamp):-1:1)/max(sdamp)).^2);
posdamp=exp(-(sdamp/max(sdamp)).^2);
damp=[negdamp,ones(size(1:nfft-2*length(sdamp))),posdamp];
damp=1;
%===========================================================
u0=U;
v0=V;
u=u0;
v=v0;
```

```matlab
vel=-2;
count=0;
dist=0;
mm=0;
nn=0;
threeu=(zeros([round(length(z)/step)+1,nfft]));
threev=(zeros([round(length(z)/step)+1,nfft]));
threeuv=(zeros([round(length(z)/step)+1,nfft]));
nmax = round(length(z)/step)+1;

for ii=1:nmax
    dist
    %figure(1),
plot(s,abs(u).^2,'b',s,abs(v).^2,'r',s,abs(u0).^2,'b:',s,abs(v0).^2,'r:')
    %pause(0.01)
    for jj=1:step
        dist=dist+dz;
    [u,v]=BPM_FracSolFiberLaser(u,v,w,dz,damp,alph,vel);
    end
    mm=mm+1;

    Pu(mm) = trapz(abs(u).^2)*ds;
    Pv(mm) = trapz(abs(v).^2)*ds;
    peaku(mm) = max(abs(u).^2);
    peakv(mm) = max(abs(v).^2);
    M(mm)=i*sum(u.*ifft(i*w.*fft(conj(u)))+v.*ifft(i*w.*fft(conj(v))))*ds;
    threeu(mm,:) = u;
    threev(mm,:) = v;
    Eu = sum(abs(u(nfft/2:end)).^2)*ds;
    Ev = sum(abs(v(1:nfft/2)).^2)*ds;
    Tu(mm) = 1/Eu*sum(s.*abs(u).^2)*ds;
    Tv(mm) = 1/Ev*sum(s.*abs(v).^2)*ds;

end
dist = z(1:step:length(z));
SP=round(L/(step*dz*60));
figure(2)
pos2 = [0.22 0.55 0.7 0.3];
subplot('position',pos2)
plot(dist,Pu,'b-',dist,Pv,'r-'),ylabel('$E$','rot',0)%,xlabel('$z
[\mathrm{m}]$')
legend('$u$-soliton','$v$-soliton','Location','southwest')
pos2 = [0.22 0.13 0.7 0.3];
subplot('position',pos2)
plot(dist,real(M),'r-'),ylabel('$\mathrm{Momentum}$'),xlabel('$z$')
%dist*xi,real(M),'b-',dist*xi,imag(M),'k-',dist*xi,
xlim([0 dist(end)])

%xL=44; xR=nx-44+2;
figure(3),
axh = axes;
waterfall(s(1:2529),dist(1:SP:end),abs(threeu(1:SP:end,1:2529)).^2), %
257:5377(1:2529) (545:1:1345) (705:1:1345) (385:1:1665) (1729:2369)
grid off, pbaspect([1 1 0.3])
xlabel('$\tau$'), ylabel('$z$'),  zlabel('$|u|^{2}$','rot',0),
azimuth = -45;
```

```matlab
elevation = 35.264;
view(axh,azimuth,elevation);
camproj
unitx = [1;0;0];
unity = [0;1;0];
unitz = [0;0;1];
projectedunitx = rotx(elevation) * rotz(-azimuth) * unitx;
projectedunity = rotx(elevation) * rotz(-azimuth) * unity;
xlabelangle = atan2d(projectedunitx(3),projectedunitx(1)); %#ok
xlabelangle = 29.9998;
ylabelangle = -(180 - atan2d(projectedunity(3),projectedunity(1))); %#ok
ylabelangle = -29.9998;
xlabelhandle = axh.XLabel;
ylabelhandle = axh.YLabel;
xlabelhandle.Rotation = xlabelangle;
ylabelhandle.Rotation = ylabelangle;
xlimits = xlim(axh);
ylimits = ylim(axh);
zlimits = zlim(axh);
xmean = mean(xlimits);
ymean = mean(ylimits);
xbottom = xlimits(1);
ybottom = ylimits(1);
zbottom = zlimits(1);
xlabelhandle.Position = [xmean ybottom zbottom];
ylabelhandle.Position = [xbottom ymean zbottom];

figure(4),
axh = axes;
waterfall(s(1:2529),dist(1:SP:end),abs(threev(1:SP:end,1:2529)).^2),
%(449:2529)
grid off, pbaspect([1 1 0.3])
xlabel('$\tau$'), ylabel('$z$'),  zlabel('$|v|^{2}$','rot',0),
azimuth = -45;
elevation = 35.264;
view(axh,azimuth,elevation);
camproj
unitx = [1;0;0];
unity = [0;1;0];
unitz = [0;0;1];
projectedunitx = rotx(elevation) * rotz(-azimuth) * unitx;
projectedunity = rotx(elevation) * rotz(-azimuth) * unity;
xlabelangle = atan2d(projectedunitx(3),projectedunitx(1)); %#ok
xlabelangle = 29.9998;
ylabelangle = -(180 - atan2d(projectedunity(3),projectedunity(1))); %#ok
ylabelangle = -29.9998;
xlabelhandle = axh.XLabel;
ylabelhandle = axh.YLabel;
xlabelhandle.Rotation = xlabelangle;
ylabelhandle.Rotation = ylabelangle;
xlimits = xlim(axh);
ylimits = ylim(axh);
zlimits = zlim(axh);
xmean = mean(xlimits);
ymean = mean(ylimits);
xbottom = xlimits(1);
```

```matlab
ybottom = ylimits(1);
zbottom = zlimits(1);
xlabelhandle.Position = [xmean ybottom zbottom];
ylabelhandle.Position = [xbottom ymean zbottom];

figure(5),pos2 = [0.22 0.55 0.7 0.3];
subplot('position',pos2)
plot(s,abs(u).^2,'b',s,abs(v).^2,'r',s,abs(u0).^2,'b:',s,abs(v0).^2,'r:')
xlabel('$\tau$'),%ylabel('Intensity')%,xlim([-15 15])

figure(6)
pos2 = [0.22 0.55 0.7 0.3];
subplot('position',pos2)
plot(dist,peaku,'b-',dist,peakv,'r-
'),%ylabel('$\mathrm{Energy[pJ]}$')%,xlabel('$z [\mathrm{m}]$')
legend('$u$-soliton','$v$-soliton','Location','southwest')

figure(7),subplot(211),
plot(s,abs(u),'b',s,abs(v),'r',s,abs(u0),'b:',s,abs(v0),'r:')
xlabel('$\tau$'),ylabel('$\mathrm{Intensity}$')%,xlim([-15 15])
subplot(212), plot(dist,unwrap(Tu),'b-',dist,unwrap(Tv),'r-')
ylabel('Position'),xlabel('$z$')

%===== Calculation of the frequency chirp ==========

phi_u = unwrap(angle(threeu(end,:)));
chirp_u = -Diff2nd(s,phi_u);
phi_v = unwrap(angle(threev(end,:)));
chirp_v = -Diff2nd(s,phi_v);

figure(8),
pos1 = [0.1 0.6 0.35 0.35];
subplot('position',pos1)
plot(s,chirp_u,'--k',s,abs(threeu(end,:)).^2,'b'), xlim([-62.4 -60.2]),
ylim([-1 2])
xlabel('$\tau$'), text(-61.1,1,'$|u|^{2}$'),text(-61.5,-0.5,'$C(\tau)$')
pos2 = [0.55 0.6 0.35 0.35];
subplot('position',pos2)
plot(s,chirp_v,'--k',s,abs(threeu(end,:)).^2,'b'), xlim([8 10.35]), ylim([-
1 2])
xlabel('$\tau$'), text(8.6,1.4,'$|u|^{2}$'),text(9,-0.5,'$C(\tau)$')
pos3 = [0.1 0.15 0.35 0.35];
subplot('position',pos3)
plot(s,chirp_v,'--k',s,abs(threev(end,:)).^2,'r'), xlim([-63.1 -59.8]),
ylim([-1 2])
xlabel('$\tau$'), text(-62.1,1.4,'$|v|^{2}$'),text(-62,-0.5,'$C(\tau)$')
pos4 = [0.55 0.15 0.35 0.35];
subplot('position',pos4)
plot(s,chirp_v,'--k',s,abs(threev(end,:)).^2,'r'), xlim([8 10.35]), ylim([-
1 2])
xlabel('$\tau$'), text(8.7,1,'$|v|^{2}$'),text(9,-0.5,'$C(\tau)$')


figure(9),
pos1 = [0.1 0.6 0.35 0.35];
subplot('position',pos1)
```

```
plot(s,chirp_u,'--k',s,abs(threeu(end,:)).^2,'b'), xlim([-21.35 -20.65]),
ylim([-10 8])
xlabel('$\tau$'), text(-20.92,5,'$|u|^{2}$'),text(-21,-5,'$C(\tau)$')
pos2 = [0.55 0.6 0.35 0.35];
subplot('position',pos2)
plot(s,chirp_v,'--k',s,abs(threev(end,:)).^2,'r'), xlim([-21.4 -20.7]),
ylim([-10 8])
xlabel('$\tau$'), text(-20.92,5,'$|v|^{2}$'),text(-21.2,-5,'$C(\
```

Calling a function

```
 function [u,v]=BPM_FracSolFiberLaser(u,v,w,dz,damp,alph,vel)

linearFrac = exp(1i/2*(abs(w).^(alph))*dz/2);
XPMu=abs(u).^2+2*abs(v).^2;
XPMv=abs(v).^2+2*abs(u).^2;
movFac = exp(-1i*vel*w*dz);

u = ifft(fft(u).*linearFrac);
v = ifft(fft(v).*linearFrac);

u = u.*exp(-1i*(XPMu)*dz);
v = v.*exp(-1i*(XPMv)*dz);

u = ifft(fft(u).*linearFrac);
v = ifft(fft(v).*linearFrac);

v = ifft(fft(v).*movFac);
u=u;
v=v;
```

Numerical Differentiation for the second derivative

Calling a function

```
function [ddfx] = Diff2nd(x,fx)

dx = x(2) - x(1);
n = length(x);

ddfx(1) = (2*fx(1)+-5*fx(2)+4*fx(3)-fx(4))/(dx^2);
ddfx(2) = (2*fx(2)+-5*fx(3)+4*fx(4)-fx(5))/(dx^2);

for j = 3:n-2
    ddfx(j) = (-fx(j+2)+16*fx(j+1)-30*fx(j)+16*fx(j-1)-fx(j-2))/(12*dx^2);
end
ddfx(n-1) = (2*fx(n-1)-5*fx(n-2)+4*fx(n-3)-fx(n-4))/(dx^2);
ddfx(n)   = (2*fx(n)-5*fx(n-1)+4*fx(n-2)-fx(n-3))/(dx^2);
```

Manuscript (Journal)

STUDIES IN APPLIED MATHEMATICS WILEY

SPECIAL ISSUE ARTICLE

Advances in the mathematics and physics of solitons in memory of David Kaup

Interactions between fractional solitons in bimodal fiber cavities

Tandin Zangmo[1] | Thawatchai Mayteevarunyoo[1] |
Boris A. Malomed[2,3]

[1]Department of Electrical and Computer Engineering, Faculty of Engineering, Naresuan University, Phitsanulok, Thailand

[2]Department of Physical Electronics, School of Electrical Engineering, Faculty of Engineering, and the Center for Light-Matter University, Tel Aviv University, Tel Aviv, Israel

[3]Instituto de Alta Investigación, Universidad de Tarapacá, Arica, Chile

Correspondence
Thawatchai Mayteevarunyoo, Department of Electrical and Computer Engineering, Faculty of Engineering, Naresuan University, Phitsanulok 65000, Thailand.
Email: thawatchaim@nu.ac.th

Dedicated to the memory of Professor David J. Kaup (1939–2022)

Abstract
We introduce a system of fractional nonlinear Schrödinger equations (FNLSEs) which model the copropagation of optical waves carried by different wavelengths or mutually orthogonal circular polarizations in fiber-laser cavities with the effective fractional group-velocity dispersion (FGVD), which were recently made available to the experiment. In the FNLSE system, the FGVD terms are represented by the Riesz derivative, with the respective Lévy index (LI). The FNLSEs, which include the self-phase-modulation (SPM) nonlinearity, are coupled by the cross-phase-modulation (XPM) terms, and separated by a group-velocity (GV) mismatch (*rapidity*). By means of systematic simulations, we analyze collisions and bound states of solitons in the XPM-coupled system, varying the LI and GV mismatch. Outcomes of collisions between the solitons include rebound, conversion of the colliding single-component solitons into a pair of two-component ones, merger of the solitons into a breather, their mutual passage leading to excitation of intrinsic vibrations, and the elastic interaction. Families of stable two-component soliton bound states are constructed too, featuring a rapidity which is intermediate between those of the two components.